CAPITAL UNIVERSITY OF SCIENCE AND TECHNOLOGY, ISLAMABAD

Numerical Analysis of Thermal Energy Flow and Substance Migration in a Domain Partially Occupied by Permeable Structures

by

Sayeda Rubab Gillani

A thesis submitted in partial fulfillment for the degree of Master of Philosophy

in the

Faculty of Computing
Department of Mathematics

2025

I honor my thesis to

my beloved family, especially

The woman who gave me life (Salma Gillani),

an aristocratic and strong person who taught me to believe in Allah,

have faith in the power of hard work, and the idea that a little can accomplish a lot.

CERTIFICATE OF APPROVAL

Numerical Analysis of Thermal Energy Flow and Substance Migration in a Domain Partially Occupied by Permeable Structures

by

Sayeda Rubab Gillani

(Registration No: MMT231003)

Thesis Evaluation Panel

S. No.	Examiner	Name	Organization
(a)	External Examiner	Dr. Qazi Mahmood Hassan	University of Wah, Wah
(b)	Internal Examiner	Dr. Rashid Ali	CUST, Islamabad
(c)	Supervisor	Dr. Muhammad Sabeel Khan	CUST, Islamabad

Dr. Muhammad Sabeel Khan
Thesis Supervisor
April-2025

Dr. Muhammad Sagheer
Head
Dept. of Mathematics
April-2025

Dr. M. Abdul Qadir
Dean
Faculty of Computing
April-2025

Author's Declaration

Under the title "**Numerical Analysis of Thermal Energy Flow and Substance Migration in a Domain Partially Occupied by Permeable Structures**," I,**Sayeda Rubab Gillani** conducted this research independently. The work is entirely original and has not been submitted for academic credit at Capital University of Science and Technology, Islamabad, or any other higher education institution, either within Pakistan or internationally.

University maintains the right to cancel my MPhil degree if this declaration is ever shown to be untrue, even after I have earned my degree.

(Sayeda Rubab Gillani)

Registration No. MMT231003

Plagiarism Undertaking

I affirm that the research contained in my MPhil thesis, titled "**Numerical Analysis of Thermal Energy Flow and Substance Migration in a Domain Partially Occupied by Permeable Structures**" is entirely my own work. Any minor support received has been appropriately acknowledged and the thesis as a whole represents the product of my independent research.

I acknowledge the strict anti-plagiarism policies of the Higher Education Commission (HEC) and Capital University of Science and Technology. As the author of this thesis, I affirm that all research presented within this document is original and that any borrowed ideas or information have been appropriately cited and attributed to their respective sources.

I declare that if any formal plagiarism is discovered in the aforementioned thesis, even after the award of my MPhil degree, the University reserves the right to revoke or withdraw my degree. Furthermore, I understand that both HEC and the University hold the authority to publish my name on their respective websites, listing individuals who have submitted plagiarized work.

(Sayeda Rubab Gillani)

Registration No. MMT231003

Acknowledgement

In the name of **ALLAH**, the Most Gracious and Merciful, who blessed humanity with the wisdom and knowledge to explore the mysteries of the universe after bringing it into existence. I would like to express my sincere appreciation and admiration for the guidance and support provided by **Dr. Muhammad Sabeel Khan**, for his constant encouragement, willingness to mentor, and invaluable help during this study process. His helpful criticism, both verbal and written, has been crucial in improving and polishing this thesis.

All of my instructors are in my sincere gratitude for their support and steadfast dedication to advancing mathematical brilliance. I also acknowledge with gratitude CUST for offering a helpful and engaging environment that made my research activities much easier.

Additionally, I wish to express my profound gratitude to my parents and my entire family from the bottom of my heart. My deepest gratitude also goes out to my fellow CUST researchers for their insightful conversations and contributions to this effort. Because of their cooperation and the supportive, stimulating atmosphere, our trip was very rewarding.

(Sayeda Rubab Gillani)
Registration No: MMT231003

Abstract

In this thesis, thermal analysis of thermal energy flow and substance migration in a domain partially filled permeable material is carried out. In this respect, a mathematical model based on the Darcy-Forchheimer model is use for modeling the dynamical characteristics in the porous medium considered. At the interface between the two subdomains, the continuity conditions are integrated with the governing partial differential equations. The governing set of PDEs are non-dimensionalzied and weak formulation of the strong form is calculated. The weak formulation of the strong form of the PDEs together with the associated boundary and interface conditions is then implemented in FreeFEM++ open source code. FreeFEM++, which is built on the finite element method, is well-suited for our study as it efficiently handles nonlinear PDEs. Numerical simulations are performed for different associated physical parameters. Results are computed in both the sub-regions of the computational domain. Profiles of the velocity and temperature fields are plotted and discussed in detail. Some interesting observations are found and stated in the conclusion section.

Contents

List of Figures

List of Tables

Abbreviations

CFD Computational Fluid Dynamics

NSD Navier-Stokes/Darcy Model

NSF Navier-Stokes/Forchheimer Model

Symbols

u_f	velocity of fluid
θ	temperature
u_p	velocity of porous medium
p_f	pressure of fluid
p_f	pressure of porous medium
t	time
$\nabla.$	divergence
∇	gradient operator
Δ	laplace operator
ρ	density
μ	dynamic viscosity
U	characteristics velocity
L	characteristics length
K	Permeability coefficient
C_F	inertial resistance coefficient
n_f, n_p	unit normal vectors
α_{BJ}	constant
p_v	viscous
p_i	inertial resistance
θ_∞	ambient temperature
θ_w	wall temperature
w_τ	tengential component
u_{pois}	pouiseuille velocity.
λ	porosity parameter

h	length of each finite element subinterval
ϕ_i	basis functions
Pr	prandtl number
Re	reynolds number
Re_p	reynold number in porous domain
Re_f	reynold number in fluid domain
Υ_h	triangulation
Gr	grashof number
W_h	Velocity-approximating finite element spaces
Q_h	Pressure-approximating finite element spaces
β	positive constant
Ω	computational domain

Chapter 1

Introduction

The interaction of thermal energy transport and substance migration in complex domains is a subject of significant interest in various scientific and engineering applications. These include geothermal energy extraction, groundwater contamination, oil recovery, biological tissue modeling, and the design of advanced heat exchangers. A notable complexity in many such systems arises when the domain under study is only partially occupied by permeable structures, such as porous media or engineered materials with selective permeability. In these cases, understanding and accurately predicting the coupled behavior of heat flow and substance transport requires robust mathematical models and efficient numerical methods.

Permeable domains present significant complexities due to their heterogeneous structure, which affects flow resistance, heat conduction, and diffusion processes. Moreover, the coexistence of free-flow and porous subdomains necessitates interface conditions that ensure physically meaningful coupling of variables such as temperature, concentration, and velocity. The coupling between thermal effects and substance transport further complicates the system, particularly when the material properties vary spatially or depend on the transported quantities.

This thesis focus on the development and analysis of numerical methods for simulating thermal energy flow and substance migration in a domain that is partially occupied by permeable structures. We adopt a coupled modeling approach that accounts for the interaction between the fluid dynamics, heat transfer, and mass

transport across both free-flow and porous regions. The ultimate goal is to provide a mathematically sound and computationally efficient framework that can handle realistic scenarios of interest in environmental and engineering contexts.

The study of flow and transport in porous media has a long and rich history, with foundational work tracing back to Darcy's law in the mid-19th century. Classical models sucsh as the Darcy and Brinkman equations have been widely used to describe flow within porous structures, while the Navier–Stokes equations govern the fluid behavior in free-flow regions. Coupling these systems across interfaces has been explored through various interface conditions, including the Beavers–Joseph–Saffman condition for velocity and continuity of temperature and solute transport across the interface. The calculation of discharge rate, velocity, and total discharge through porous media is analyzed using Darcy's law, with a particular focus on the role of porosity in water retention [1], the study highlights the role of porosity in porous media's ability to retain or allow water flow, offering insights into their use for water conservation or seepage control in applications like earth dams. An examination of heat and moisture interactions across a porous interface reveals how both factors are generated simultaneously in certain systems. As heat accumulates, moisture—whether from condensation or other processes migrates through the porous structure and evaporates into the surrounding environment. This evaporation absorbs heat, helping regulate the system's internal temperature. The findings emphasize the essential role of porous materials in managing both heat and moisture, providing valuable insights for thermal management in applications like wearable systems and ventilation jackets [2, 3]. The effectiveness of this mechanism depends on multiple factors, including the material's porosity, ambient temperature, humidity levels, and the intensity of the heat source. A higher-order Darcy-Forchheimer model is developed to investigate non-linear flow in highly permeable media under temperature boundary conditions, with the solution obtained through finite element methods [4]. This approach helps in understanding how factors such as Grashhoff and Forchheimer numbers, along with porosity, affect the thermal flow this helps in understanding how permeability and flow transitions are affected by the medium, which is useful for improving interface modeling in porous regions dynamics. From this, it

becomes clear that understanding these factors is essential for enhancing thermal performance in porous media systems. Samelike relevant study focuses on natural convection of power-law fluids within porous enclosures, emphasizing how porosity, fluid properties, and thermal conditions affect heat transfer. Finite element analysis is used to examine the resulting flow and temperature distribution [5]. It is observed that porosity strongly influences the thermal gradients and flow patterns, making it a critical factor in enhancing heat transfer within porous media. A CFD-based study on power-law fluid flow through isotropic porous media reveals that the structure of the medium plays a dominant role in shaping flow behavior [6]. It highlights a coupling between fluid viscosity and porous geometry, leading to a transition between Newtonian and non-Newtonian regimes. This helps in understanding how permeability and flow transitions are affected by the medium, which is useful for improving interface modeling in porous regions. The investigation conducted through pore-scale numerical simulations explores convective flow in porous media, focusing on how porosity influences the transition between the Darcy and Rayleigh Bénard regimes. The results reveal that as porosity increases, the scaling exponent of the Sherwood number and Rayleigh Darcy number decreases in the Darcy regime, emphasizing the role of porosity in heat and mass transfer processes [7]. This insight is valuable for understanding how porosity affects convection patterns, offering new perspectives on the limitations and validity of the Darcy model in porous media.

The investigation explores the fluid dynamics involved in heat transfer, with the goal of identifying potential modeling approaches to describe the complicated physical characteristics of the system. Through focusing on the intricate interactions between fluid movement, thermal energy transfer, and material characteristics, research lays the groundwork for developing a more comprehensive model that can account for additional factors, such as the effects of heat and sweat on the overall system dynamics. The insights gained from this study not only enhance our understanding of the specific application at hand but also provide valuable methodologies that could be adapted across a wide spectrum of scenarios. These contain various industrial, environmental, and biomedical applications based on fluid movement within saturated porous media. Whether it involves improving the

efficiency of thermal management systems, optimizing filtration processes [8], or advancing medical treatments rely on controlled fluid dynamics, the modeling and simulation approaches developed here offer a versatile toolkit. This research is a foundational step toward bridging the gap between theoretical modeling and practical applications, ultimately contributing to the design of more effective systems in diverse fields. The distinct physical characteristics of the fluid and permeable structure regions necessitate the use of separate mathematical models for each. This results in a combined, heterogeneous model that accounts for the unique behaviors of both regions. While the Navier-Stokes equations are commonly used to describe free-fluid flows, porous medium flows require specialized models. Darcy's law offers a straightforward approach [9], whereas high-permeability media often demand the more complex nonlinear Forchheimer equation. The investigation explores the fluid dynamics involved in heat transfer, aiming to identify potential modeling approaches to capture the complex physical characteristics of the system. By focusing on the intricate interactions between fluid movement, thermal energy transfer, and material properties, the research lays the foundation for developing a more comprehensive model that incorporates additional factors, such as the effects of heat and sweat on the overall system dynamics [10]. The fluid behavior is modeled using the Navier-Stokes equations, which govern the motion of viscous fluids, allowing for a detailed representation of the convection processe within the system. The study [11] investigates two methods for modeling fluid filtration through porous media: applying the full Navier-Stokes equations with porous medium terms and solving the fluid and porous regions separately with interface conditions. An iterative algorithm for a Navier–Stokes/Forchheimer problem is presented, with applications to motorbike helmet ventilation. The findings aid in refining simulation approaches for fluid-porous media interactions in practical scenarios.

After reviewing previous studies and literature, this thesis develops a comprehensive approach for analyzing thermal energy flow and substance migration in domains partially filled with permeable materials. A mathematical model based on the Navier-Stokes-Forchheimer equations, combined with Darcy's law, is formulated to capture the dynamic behavior of the system. Thermal effects are

incorporated into the governing equations, allowing for the simulation of fluid flow and temperature fields within the porous medium. These equations, along with boundary and interface conditions, are solved using the FreeFEM++ open-source software, which is well-suited for handling nonlinear partial differential equations. Numerical simulations are performed for various physical parameters, providing in-depth analysis of the temperature and velocity profiles, leading to key insights into the thermal behavior in porous media. Furthermore, this thesis advances existing theoretical and numerical methodologies by applying advanced finite element techniques, decomposing the problem into manageable components, and utilizing iterative coupling strategies to analyze coupled thermal and substance transport in heterogeneous domains. After reviewing previous studies and literature, this thesis develops a comprehensive approach for analyzing thermal energy flow and substance migration in domains partially filled with permeable materials. A mathematical model based on the Navier-Stokes-Forchheimer equations, combined with Darcy's law, is formulated to capture the dynamic behavior of the system. Thermal effects are incorporated into the governing equations, allowing for the simulation of fluid flow and temperature fields within the porous medium. These equations, along with boundary and interface conditions, are solved using the FreeFEM++ open-source software, which is well-suited for handling nonlinear partial differential equations. Numerical simulations are performed for various physical parameters, providing in-depth analysis of the temperature and velocity profiles, leading to key insights into the thermal behavior in porous media. Furthermore, this thesis advances existing theoretical and numerical methodologies by applying advanced finite element techniques, decomposing the problem into manageable components, and utilizing iterative coupling strategies to analyze coupled thermal and substance transport in heterogeneous domains.

1.1 Thesis Accomplishments

In this research, a comprehensive analysis of two distinct methods is performed by investigating their mathematical formulations and finite element approximations.

The Navier-Stokes equations are employed within this study to model fluid dynamics, the thermal energy equation to capture heat transfer, and applies Darcy's law for linear fluid movement through permeable substances, while the Forchheimer equation is employed for non-linear flow scenarios. A detailed mathematical model is created as partial differential equations (PDE's), with calculations carried out through tensor calculus. The governing equations are transformed into their weak form, and a finite element model is derived, which is then implemented using the numerical software FreeFEM++ (http://freefem.org/). The developed code is used to perform simulations, analyze the data, and generate results that are systematically tabulated, ensuring mesh independence of the solution. Finally, the outcomes are presented and discussed in relation to varying physical parameters of interest, offering insights into the efficiency of the techniques in modeling heat transfer through porous media.

1.2 Outcomes

This research yields the following results:

- Develop the mathematical model that is useful for studying and integrate the Navier-Stokes equation(NSE), Darcy's law, and Forchheimer equation with thermal energy equation for dealing with partially filled porous cavities.
- Formulate the weak form of the formulated model to compute thermal conduction through a partially filled permeable structure.
- Implement the weak formulation based on finite elements in the open-source code FreeFEM++.
- Compute the flow and thermal characteristics through partially filled porous medium.
- Analyze the results obtained through the performed simulations.

.

1.3 Thesis Layout

The structure of this thesis includes the subsequent chapters.

- **Chapter 2** covers the fundamental principles of fluid dynamics, providing a concise overview of essential definitions, the governing laws of fluid motion, and the relevant equations. It also briefly discusses dimensionless physical quantities pertinent to the problems at hand.

- **Chapter 3**, The study explores the differential-based approach governing fluid motion and saturated porous media flow [12]. A thorough analysis of the underlying equations and their physical interpretations is provided, ensuring a comprehensive understanding of the mechanics involved. Additionally, the coupling conditions required for handling heterogeneous cases, where different flow regimes interact, are discussed. This section also presents suitable dimensional formulations that simplify the models, making them more accessible for numerical treatment and comparison.

- In **Chapter4**,The focus shifts to the numerical approximation of these models, examining the chosen finite element method and discussing its advantages and challenges. This section also presents potential solution strategies for the space-temporal division of the problems, taking into account factors like accuracy, stability, and computational efficiency. By analyzing the chosen discretization approach, the goal is to provide insights into the most effective way to tackle complex simulations in practical applications.

- **Chapter 5** the non-linear Navier–Stokes/Forchheimer model is presented along with numerical results. The simulation outcomes are displayed, offering a detailed comparison of results derived from different modeling ap-

proaches. Each technique's accuracy and efficiency are assessed, supported by both visual representations and quantitative data. Additionally, graphs and diagrams are provided to illustrate how temperature changes and responds to the effects of Reynolds number (Re), inertial resistance coefficient C_F, Prandtl number (Pr), and permeability (K), enhancing the clarity of the findings.

Chapter 2

Basic Principles

The basic ideas and concepts that underline flow dynamics are introduced in this chapter, including:

1. Key Clarifications
2. Fundamental laws
3. Dimensional Parameters
4. Key quantities

Gaining a thorough understanding of the subjects covered in the upcoming chapters requires mastering these fundamentals.

2.1 Key Clarifications

2.1.1 Thermophysical Properties

2.1.1.1 Mass Density or Density

"Density (ρ) is defined as the mass per unit volume of a substance" [13]. Mathematically, it is expressed as

$$\rho = \frac{m}{V},$$

where

- ρ is the density (kg/m^3 in SI units),
- m is the mass of the substance (kg),
- V is the volume of the substance (m^3).

This fundamental equation is widely used in physics and engineering to describe the compactness of a material.

2.1.1.2 Viscosity

"Kinematic viscosity (ν) is a measure of a fluid's resistance to flow under the influence of gravity. It is defined as the ratio of dynamic viscosity (μ) to density (ρ)" [14], expressed as:

$$\nu = \frac{\mu}{\rho},$$

where

- ν is the kinematic viscosity (m$^\mathbf{2}$/s),
- μ is the dynamic viscosity (Pa·s or N·s/m$^\mathbf{2}$),
- ρ is the fluid density (kg/m$^\mathbf{3}$).

This property is important in fluid mechanics as it determines how easily a fluid flows without considering external forces. Imagine a river flowing through a narrow channel. If the water is clear and moves swiftly, it indicates low kinematic viscosity, meaning it can flow easily without much resistance. However, if mud or silt is mixed into the water, the flow slows down because the mixture has a higher kinematic viscosity, making it more resistant to motion.

2.1.1.3 Pressure

"Pressure (P) is defined as the force exerted per unit area on a surface." [15] It quantifies how much force is applied over a specific area and is expressed mathematically as:

$$P = \frac{F}{A},$$

where

- P is the pressure (Pa or $\mathrm{N/m^2}$),
- F is the applied force (N),
- A is the surface area over which the force is distributed ($\mathrm{m^2}$).

Pressure plays a crucial role in fluid mechanics, thermodynamics, and engineering applications, influencing fluid behavior in pipes, hydraulic systems, and atmospheric studies.

2.1.1.4 Permeability

"Permeability (K) is a measure of a material's ability to allow fluids to pass through it. It describes how easily a fluid can move through a porous medium and is an essential parameter in fields such as hydrogeology, petroleum engineering, and soil mechanics". [16]

Permeability depends on factors such as the size and connectivity of pores within a material. Highly permeable materials like sand allow water to flow easily, while low-permeability materials like clay restrict fluid movement.

2.1.1.5 Inertial Resistance

"Inertial resistance refers to the resistance encountered by a fluid due to its inertia when flowing through a porous medium or an obstacle. It becomes significant at higher flow velocities and is commonly represented using the inertial resistance

coefficient (C_F), which accounts for the non-linear dependence of pressure drop on velocity. This parameter is essential in modeling high-speed fluid flow in porous media and turbulent flow conditions."[17]

2.1.1.6 Pouiseuille Velocity

"The mean velocity is defined for a Newtonian fluid undergoing laminar flow through a circular pipe is called Pouiseuille velocity. It comes from the fundamentals of fluid mechanics and is important for comprehending the behavior of fluids in small areas."[18]

2.2 Dimensionless Parameters

The discussion in the upcoming chapters will include the following dimensionless numbers.

2.2.1 Reynolds Number

"The Reynolds number reflects the comparison of fluid's inertial forces along with the molecular friction, serving as a key indicator of the flow's hydrodynamic properties. Determining the type of fluid flow—laminar, transient, or turbulent—helps.For laminar flow, the Reynolds number is typically less than 2000, While transient flow occurs when $2000 < \text{Re} < 4000$, and turbulent flow sets in when Re exceeds 4000."[19]

$$Re_f = \frac{\rho U L}{\mu}.$$

The fluid's dynamic energy is quickly dampened by the viscous forces at low Reynolds numbers, avoiding significant streamline deformation and maintaining the smooth, ordered (laminar) flow. Higher Reynolds numbers, however, cause the inertial forces to take over and overcome the viscous resistance. This imbalance

leads to the loss of flow stability, marked by the formation of eddies and turbulence within the fluid. In such cases, the flow becomes irregular and chaotic as the viscous forces can no longer counteract the momentum-driven disturbances.

2.2.2 Grashof Number

"In the presence of buoyancy forces, the Grashof number (Gr_n) is a dimension-independent quantity that is intended to characterize the behavior of fluid flow. It is particularly helpful for examining natural convection phenomena because it contrasts the impact of buoyant forces with the viscous forces within a fluid." [20, 21]

The Grashof number in its dimensionless form is given by:

$$Gr_n = \frac{\rho K L}{\mu L},$$

where

- ρ refers to the fluid density
- K refers to a characteristic property (such as thermal diffusivity or permeability depending on context)
- L is defining the length scale
- μ is defining as dynamic viscosity

Grashof number related to inertial resistance (Gr_f) is used to express the comparison between inertial forces relative to viscous forces inside a porous medium. It's especially helpful for explaining fluid flow through media when inertial resistance and permeability are important factors. Mathematically, it is given as:

$$Gr_f = \frac{\rho C_F U \sqrt{K}}{\mu},$$

where

- ρ indicates the density of the fluid
- C_F is defining as inertial resistance coefficient
- U is the fluid velocity
- K represents permeability
- μ is defining as the dynamic viscosity

The Grashof number in this form is more effective in capturing the influence of inertial resistance and permeability on flow characteristics.

The Grashof number related to buoyant forces (Gr_c) is another dimensionless form that compares buoyant forces to the inertial forces within a porous medium, with emphasis on the impact of material properties like permeability and thermal expansion. It is expressed as:

$$Gr_c = \frac{\alpha_{BJ} L}{\sqrt{K}},$$

where

- α_{BJ} is a constant that assumes values between 0.8 and 1.2
- L is a characteristic length
- K is permeability.

2.2.3 Prandtl Number

"The Prandtl number (Pr) is a unitless parameter that delineates the relative thickness of the momentum as well as thermal boundary layers within a fluid. It is a crucial component of heat transport analysis, especially when convection is included." [18] The Prandtl number can be expressed mathematically as follows:

$$Pr = \frac{\mu C_p}{K},$$

here

- μ signifies the fluid's dynamic viscosity
- C_p represents the thermal capacity per unit mass at constant pressure,
- K signifies the fluid's heat conductance.

In basic terms, the Prandtl number measure the proportion of thermal diffusivity (driven by thermal factors) to momentum diffusivity (affected by viscous forces).

When thermal diffusion is more prominent than momentum diffusion, heat can spread more quickly than momentum when the Prandtl number is below unity, which is usually less than 1.This phenomenon is frequently observed in liquid metals.

In contrast, a Prandtl number exceeding unity (greater than 1) implies that momentum diffusion prevails over thermal diffusion, suggesting that the fluid maintains its thermal energy for a more extended period before it is transported. High-viscosity fluids, such as oils, exhibit this tendency.

2.2.4 Porosity Number

"Porosity Number is a dimensionless quantity used in fluid dynamics and porous media studies. It is defined as the ratio of the effective permeability of a material to the permeability of the fluid passing through it. The Porosity Number is often used in studies of fluid flow through porous materials, particularly when considering the relationship between permeability and the fluid's resistance to flow." [22] This number is useful in characterizing the behavior of fluids moving through porous media, as it compares how well the material allows flow relative to the fluid's intrinsic properties.

2.3 Sready and Unsteady Flow

2.3.1 Steady Flow

The term “Steady Flow” describes a situation where the fluid characteristics at any given point in the flow field are constant over time. As time passes in this scenario, variables like density, pressure, and velocity do not change at any particular moment. For example, in a system with uniform water flow in a pipe, the pressure and velocity at any given place in the pipe will not change over time. Steady flow can occur in both incompressible and compressible fluids, and it facilitates the analysis of fluid behavior, as the governing equations can be applied without accounting for temporal variations.

2.3.2 Unsteady Flow

On the other hand, temporal changes in fluid characteristics at any specified point in the flow field are indicative of unstable flow. Variables including density, pressure, and velocity can alter over time in this kind of flow. An illustrative example of unsteady flow is the scenario where water is intermittently supplied through a faucet; in this case, both the velocity as well as pressure within the pipe experience fluctuations as the faucet is opened and closed. The analysis of unsteady flow is inherently more complex, as the governing equations must incorporate time-dependent factors, necessitating consideration of time-varying boundary conditions. On the other hand, temporal changes in fluid characteristics at any specified point in the flow field are indicative of unstable flow. Variables including density, pressure, and

velocity can alter over time in this kind of flow. An illustrative example of unsteady flow is the scenario where water is intermittently supplied through a faucet; in this case, both the velocity as well as pressure within the pipe experience fluctuations as the faucet is opened and closed. The analysis of unsteady flow is inherently0.3cm more complex, as the governing equations must incorporate time-dependent factors, necessitating consideration of 0.3cmtime-varying boundary conditions.

2.4 Fundamental Laws

2.4.1 Darcy's Law

"Darcy's law is an essential concept in the theory of fluid flow through permeable medium. Fluid viscosity and the medium's permeability are taken into consideration, and a mathematical relationship between the velocity of fluid along with the driving forces in the material is provided." [22, 23] The law is represented as follows:

$$\boldsymbol{u_p} = -\frac{K}{\mu}\nabla P_p,$$

where

- u_p is Darcy velocity, indicating as average fluid velocity through the permeable structure,
- k is permeability of the medium, a measure of its ability to allow fluid to pass,
- μ is dynamic viscosity of the fluid, which governs its internal resistance to flow,
- ∇P_p is the fluid flow across the medium due to a pressure gradient.

Darcy's law establishes a linear relationship between fluid velocity and the permeability of the porous medium, while inversely correlating it with fluid viscosity. This law effectively describes a balance between the forces driving fluid flow within the medium and the inherent resistance offered by the porous structure. This equation is essential for analyzing fluid flow in porous materials, which has applications in filtration procedures, petroleum reservoir engineering, and groundwater hydrology.

2.4.2 Forchheimer Law

"Forchheimer's Law is an extension of Darcy's Law that accounts for the nonlinear effects of inertial forces in fluid flow through porous media. It is particularly applicable when the flow velocity is high, leading to deviations from the purely viscous-dominated regime described by Darcy's Law." [22, 24] Mathematically, Forchheimer's Law is expressed as:

$$\nabla P = -\left(\frac{\mu}{K}u + \rho C_F u^2\right),$$

where

- ∇P is the pressure gradient,
- μ is the dynamic viscosity of the fluid,
- K is the permeability of the porous medium,
- u is the fluid velocity,
- ρ is the fluid density,
- C_F is the Forchheimer coefficient, which accounts for inertial effects.

This law is significant in describing high-velocity flows through porous structures, such as in packed beds, groundwater movement in coarse-grained media, and petroleum reservoirs.

2.4.3 Thermal Energy

The thermal energy equation is fundamental to understanding heat transfer in fluid media. Convective and conductive heat transport methods are both taken into consideration by this equation, which regulates the conservation of thermal energy.. It is mathematically described as:

$$\rho C_p \frac{\partial \theta}{\partial t} + \mathbf{u_f} \cdot \nabla \theta = K \nabla^2 \theta.$$

Where

- ρ is the fluid density, which quantifies the mass per unit volume of the fluid,
- C_p symbolizes the specific heat capacity at normal pressure, showing how much heat is needed to raise a fluid's temperature by one degree per unit mass.,
- θ symbolizes the temperature field, describing the temperature distribution within the fluid,
- $\frac{\partial \theta}{\partial t}$ is the temporal derivative of the temperature, representing the rate of temperature change over time,
- $\mathbf{u_f}$ stands for the velocity field of the fluid, encapsulating the magnitude and direction of fluid flow,
- $\nabla \theta$ describes the spatial gradient of the temperature field, reflecting temperature variation across space,
- K is the thermal diffusivity, a material property that defines the rate at which heat diffuses through the fluid,
- $\nabla^2 \theta$ is the Laplacian of the temperature, representing the second-order spatial derivative and characterizing the diffusion of heat.

This equation establishes a balance between three key phenomena:

- Temporal changes in the temperature field $\rho C_p \frac{\partial \theta}{\partial t}$,
- Convective thermal energy transfer due to the flowing substance, represented by the term $\mathbf{u_f} \cdot \nabla \theta$,
- Conductive heat transfer, expressed by $\kappa \nabla^2 \theta$, which quantifies the diffusive transport of heat within the medium.

This equation illustrates how thermal energy is transported within the fluid through both convection, where the movement of the fluid carries heat, furthermore conduction, where heat diffuses through the material. The thermal energy equation is a fundamental tool for describing heat transport in various scientific and engineering applications, including fluid dynamics, thermodynamics, geothermal systems, as well the design of heat exchanges. It is especially important for understanding the evolution of thermal energy in fluids with shifting boundaries and for forecasting temperature fields.

2.4.4 Continuous Equation

The continuity equation, denoted as $\nabla \cdot \mathbf{u_f} = 0$, is a fundamental tenet in fluid dynamics that encapsulates the principle of mass conservation within a fluid flow regime. This equation postulates that, in the context of incompressible flow, the divergence of the fluid velocity field $\mathbf{u_f}$ is identically zero, signifying that there is no net change in mass within any designated control volume over time.

- **Incompressibility Assumption**: The continuity equation predominantly applies to incompressible fluids, where the density remains constant regardless of the flow conditions. Under this premise, any volumetric zone must have a rate of mass transfer that is equal to the mass flow rate leaving it, thereby ensuring the principle of mass conservation is upheld throughout the flow field.
- **Divergence of Velocity**: The divergence operator quantifies the rate of expansion or contraction of fluid at a specific point within the flow. A

divergence of zero implies that the fluid neither accumulates nor depletes in that locality, which is a prerequisite for steady-state flow conditions.

- **Implications in Fluid Dynamics**: This equation serves as an essential framework for the analysis and modeling of fluid motion. It establishes a robust mathematical foundation for numerous engineering applications, including, although not limited to, the flow of liquids through conduits, aerodynamic behavior around structures, moreover various fluid systems. The continuity equation serves as a crucial restriction when determining fluid velocity fields and pressure distributions in complex flow settings by stating mass conservation..

Chapter 3

Mathematical Framework of Fluid Transport within Porous Media

This chapter explores the formulation as well as algorithms related to finite element methods(FEM).Without taking thermal energy into account, the first section focuses on mathematical models for flow through a porous material, providing a foundational understanding of the problem as well as solution approaches. Extend the study in the second section to incorporate the thermal energy effects, which introduce new complications and need for altered methods for precise modeling and resolution.

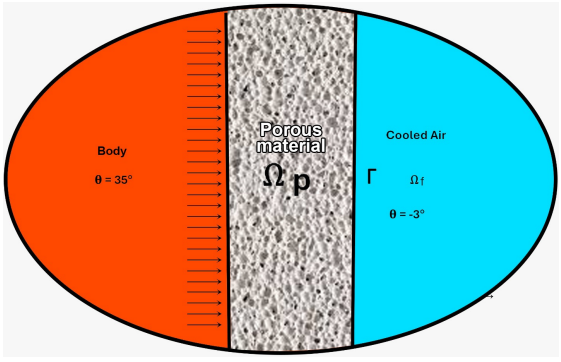

FIGURE 3.1: The domain Ω consists of two subdomains: Ω_f (fluid) and Ω_p (porous medium), with temperature Θ in Ω_p.

3.1 Navier-Stokes Forchheimer Model

We concentrate on a domain with defined boundaries Ω split into two-distinct parts such that:

$$\Omega = \Omega_f \cup \Omega_p,$$

and

$$\Omega_f \cap \Omega_p = \emptyset.$$

At which Ω_f is define as a domain containing fluid (For instance, containing water or air) and Ω_p is define as a domain of saturated porous medium. $\Gamma = \Omega_f \cap \Omega_p$ denotes the contact surface linking both regions(see Fig. 1). The interface between the confined fluid and the permeable medium, considered from a physical perspective, is mathematically described by the surface Γ.

3.1.1 Fluid Region: The Navier-Stokes Differential Equations

Inside the domain Ω_f, The Navier-Stokes differential equation are utilized to simulate a confined incompressible viscous fluid: throughout "t" is greater than zero,

$$\begin{aligned} &(\rho\frac{\partial \mathbf{u}_f}{\partial t} + (\mathbf{u}_f \cdot \nabla)\mathbf{u}_f) + \nabla p_f - \mu\nabla \cdot \nabla \mathbf{u}_f = 0 \qquad \text{in } \Omega_f, \\ &\nabla \cdot \mathbf{u}_f = 0 \qquad \text{in } \Omega_f. \end{aligned} \tag{3.1}$$

The fluid's density and dynamic viscosity are shown as ρ and μ, respectively, and it is assumed that no external body forces are acting. Furthermore, It is recalled that

$$(\mathbf{v} \cdot \nabla)\mathbf{w} = \sum_{i=1}^{d} v_i \frac{\partial \mathbf{w}}{\partial x_i},$$

for every vector fields $\mathbf{v} = (v_1, \ldots, v_d)^T$, $\mathbf{w} = (w_1, \ldots, w_d)^T$.

The Reynolds number is defined as

$$Re_f = \frac{\rho U L}{\mu}. \tag{3.2}$$

Navier-Stokes equations must incorporate turbulence models since turbulence effects, like those of the Reynolds Averaged Navier-Stokes (RANS) equation, become substantial at high Reynolds numbers. The analysis will always be conducted under the assumption of the laminar case in the applications.

3.1.2 Filtration Over the Porous Domain

Filtration through a saturated porous domain can be modeled using Darcy's equation. The most straightforward (linear) relationship in the pressure p_p and velocity u_p in a porous medium is termed the Darcy law and declared that

$$\mathbf{u}_p = -\frac{K}{\mu}\nabla p_p \quad \text{in } \Omega_p. \tag{3.3}$$

Darcy's law, a fundamental principle in fluid flow through porous media, incorporates the dynamic viscosity coefficient (μ) (previously defined in Equation 3.1) and the permeability coefficient (K) as crucial parameters. Although empirically established by Darcy in 1856 [25], this law has been rigorously supported by theoretical derivations from the Navier-Stokes equations using homogenization techniques, particularly for well-defined porous structures (e.g., [26]). The permeability coefficients exhibit significant variability, which spans several orders of magnitude, from ($10^{-5}\,\mathrm{m}^2$) in synthetic porous materials to as low as ($10^{-20}\,\mathrm{m}^2$) in certain natural formations such as soils and rocks. In anisotropic media, the scalar permeability coefficient (k) is generalized to a tensorial representation to account for directional variations in flow resistance.

There is a smooth transition to a non-linear drag as the seepage velocity rises. Compatible to the Navier-Stokes equations, Reynolds number connected to the pores can be defined to describe the significance of the inertial effects:

$$Re_p = \frac{\rho U \delta}{\mu}, \tag{3.4}$$

with δ defined as the characteristic pore size.

For values where $Re_p < 1$, the Darcy law is dependable (see, for example, [27]). If not, a more comprehensive model that takes into account the inertial effects must account into consideration, similarly the Forchheimer's nonlinear equation [28]

$$\nabla p_p = -\frac{\mu}{k}\mathbf{u}_p - \frac{\rho C_F}{\sqrt{K}}|\mathbf{u}_p|\mathbf{u}_p, \quad \text{in } \Omega_p. \tag{3.5}$$

The range $1 < Re_p < 10$ signifies the transition zone intermediate the Darcy flow regime, dominated by viscous forces, and the Forchheimer flow regime, where inertial forces become increasingly significant. Additionally, for Darcy's law, nonlinear adjustment terms of the form $|\mathbf{u_p}|^{\alpha}\mathbf{u_p}$, where $1 < \alpha < 2$, may also be incorporated. You may find a detailed examination of their physical interpretation in [29, 30]. One can homogenize the governing equations (Navier-Stokes) of fluid motion to yield the Forchheimer equation, which is the Darcy law (see [31]).

The continuity equation is taken into consideration in order to fully establish the filtration model:

$$\nabla \cdot \mathbf{u_p} = 0, \quad \text{in } \Omega_p. \tag{3.6}$$

The following elliptic equation containing only the pressure is produced by combining the latter with the Darcy equation (3.3):

$$-\nabla \cdot \left(\frac{K}{\mu}\nabla p_p\right) = 0, \quad \text{in } \Omega_p. \tag{3.7}$$

Darcy's law (3.3) can be used to retrieve the velocity if only (3.7) is solved in Ω_p.

3.1.3 Conditions of Coupling throughout the Interface

In order to demonstrate how the unconstrained fluid works, filtered across the permeable material, we must apply appropriate coupling conditions between the Darcy (or Forchheimer) and Navier–Stokes equations across their shared interface Γ. Specifically, we consider the following three circumstances.

1. Continuity of the velocity's normal component:

$$\mathbf{u}_f \cdot \mathbf{n}_f = -\mathbf{u_p} \cdot \mathbf{n}_p, \quad \text{on } \Gamma. \tag{3.8}$$

Here, the unit vectors $\mathbf{u_p}$ and $\mathbf{n_f}$ are perpendicular to the surfaces $\partial\Omega_p$ and $\partial\Omega_f$, correspondingly (see Fig. 1). On Γ, whereby $\mathbf{n}_f = -\mathbf{n}_p$. Equation (3.8) can be rewritten using Darcy's law (3.3) as follows:

$$\mathbf{u}_f \cdot \mathbf{n}_f = \frac{K}{\mu}\frac{\partial p_p}{\partial n_p}, \quad \text{on } \Gamma. \tag{3.9}$$

This state results from the incompressibility of the fluid.

2. Normal stress continuity across Γ

$$p_f - \mu\frac{\partial \mathbf{u}_f}{\partial n_f} \cdot \mathbf{n}_f = p_p, \quad \text{on } \Gamma. \tag{3.10}$$

Keep in mind that pressures could vary throughout the interface.(see, e.g.[32]):

3. To fully define the flow within the free-fluid domain, an additional boundary condition is required for the tangential component of the fluid velocity at the interface. Based on the work of Beavers and Joseph [33], a crucial condition states that the shear stress at the interface is directly proportional to the fluid slip velocity difference and the tangential component of the seepage-velocity within the porous medium.

$$-(\frac{\partial \mathbf{u}_f}{\partial n_f})_{\boldsymbol{\tau}} = \frac{\alpha_{BJ}}{\sqrt{K}}(\mathbf{u}_f - \mathbf{u}_p)_\tau, \quad \text{on } \Gamma. \tag{3.11}$$

The component of the the vector $\mathbf{v}$ tangential at interface, denoted as $(\mathbf{v})_\tau$, is expressed as.

$$(\mathbf{v})_\tau = \mathbf{v} - \mathbf{v} \cdot \mathbf{n}, \quad \text{on } \Gamma. \tag{3.12}$$

The typical values of the constant α_{BJ} fall between 0.8 and 1.2 (see [33]). Saffman suggested using the following simplified condition(also known as the Beavers–Joseph–Saffman

condition) [34] since the velocity of the seepage $\mathbf{u}_p$ at the interface is much lower than the slip velocity of fluid $\mathbf{u}_f$:

$$-(\frac{\partial \mathbf{u}_f}{\partial n_f})_{\boldsymbol{\tau}} = \frac{\alpha_{BJ}}{\sqrt{K}}(\mathbf{u}_f)_\tau, \quad \text{on } \Gamma. \tag{3.13}$$

Jäger and Mikeli [32, 35, 36] later used homogenization to derive this requirement mathematically. A thorough analysis and study of the three interfacial coupling conditions covered in this chapter can also be found in [37–42].

Remark 2.1 The Navier-Stokes equations are represented in a temporal form when we look at time-invariant flow model through a permeable media. This is supported by the fact that, because the fluid domain velocity is typically significantly higher, seepage velocity can be thought of as stable for brief periods of time. An unsteady model for Ω_p could be taken into account if this assumption is not true, as researched in studies like [43].

3.1.4 Penalization Method

The coupled model presented in previous sections poses significant computational challenges due to the inherent dissimilarity between the governing equations in the fluid (Ω_f) and porous (Ω_p) subdomains. To address it, the method of penalization has emerged as a viable approach for simulating flow across porous surfaces (see, e.g., [44], [45], [46]). This technique involves modifying the fluid flow equations across the entire computational region and incorporating two distinct resistance factors. These terms effectively account for the resistance encountered by the fluid within the porous medium (Ω_p), encompassing both non-linear Forchheimer effects (equation 3.3) and linear Darcy behavior (equation 3.5). More specifically, we analyze the momentum equation:

$$\rho\left(\frac{\partial \mathbf{u}}{\partial t} + (\mathbf{u}\cdot\nabla)\mathbf{u}\right) - \mu\nabla\cdot\nabla\mathbf{u} + \nabla p + \left(\frac{\mu}{K}\mathbf{u} + \frac{\rho C_F}{\sqrt{K}}|\mathbf{u}|\mathbf{u}\right)\chi_{\Omega_p} = 0. \tag{3.14}$$

The physical constants in these equations remain consistent with those previously defined in equations (3.1) and (3.5). The characteristic function χ_{Ω_p} is introduced,

where $\chi_{\Omega_p} = 1$ within the porous domain (Ω_p) and zero elsewhere. This ensures that the additional terms associated with porous media effects vanish in (Ω_f). The velocity variable $\mathbf{u}$ represents the actual fluid velocity within Ω_f and the seepage-velocity within the porous domain Ω_p.

Remark 2.2. The "fictitious domain" approach, first introduced in [47], has been effectively adapted to include interior solid regions within the computational domain. This method is particularly useful when addressing significant spatial variations in permeability coefficients throughout the domain, as it requires solving modified Navier-Stokes equations. Homogenization studies (e.g., [48]) have validated this approach as an accurate framework for modeling both fluid regions (where $K \to +\infty$) and solid regions (where $K \to 0$).

For the interpretation of equation (3.14), the diffusive term $(-\mu\nabla \cdot \nabla\mathbf{u})$ has been shown to accurately describe the flow behavior in materials with high porosity. This formulation is commonly referred to as the Brinkman-Forchheimer equation (see [49], [26]), often assuming $\tilde{\mu} = \mu$. However, the convective term $(\mathbf{u} \cdot \nabla)\mathbf{u}$ which is nonlinear has faced criticism for inadequately capturing nonlinear effects due to inertia. For example, in constant, incompressible unidirectional flows, this term becomes negligible regardless of the velocity $\mathbf{u}$, which is not consistent with physical expectations. Despite its limitations, the penalization method continues to be widely used in commercial simulation software because of its simplicity compared to the coupled methods discussed in Section 3.1.3. Many commercial packages designed to simulate flows in partially filled porous media domains rely on this method (e.g., [50], [51], [52]). These tools typically define two constants, P_v and P_i, to characterize the permeable medium in the domain Ω_p. These constants, which are non-zero only within the porous region, account for viscous and inertial resistance, respectively. The modified Navier-Stokes equations that incorporate these penalization terms are then solved numerically.

$$\rho\left(\frac{\partial \mathbf{u}}{\partial t}+(\mathbf{u}\cdot\nabla)\mathbf{u}\right)-\mu\nabla\cdot\nabla\mathbf{u}+P_i|\mathbf{u}|\mathbf{u}+P_v\mathbf{u}+\nabla p=0 \quad \text{in}\Omega,$$
$$\nabla\cdot\mathbf{u}=0 \quad \text{in } \Omega. \tag{3.15}$$

where

$$P_v=\begin{cases}0 & \text{in } \Omega_f\\ \frac{\mu}{K} & \text{in } \Omega_p,\end{cases} \quad \text{and} \quad P_i=\begin{cases}0 & \text{in } \Omega_f\\ \frac{\rho C_F}{\sqrt{K}} & \text{in } \Omega_p.\end{cases} \tag{3.16}$$

3.1.5 Dimensionless Formulations

In order to facilitate comparison, we present the dimensionless forms of the models we have examined. The dimensionless variables can be expressed as follows: To facilitate a comparison between the models, we will express them in dimensionless form. To this end, To proceed, we specify the relevant non-dimension variables:

$$t'=\frac{U}{L}t, \quad \mathbf{X}'=\frac{\mathbf{x}}{L}, \quad \mathbf{u}'_f=\frac{\mathbf{u}_f}{U}, \quad \mathbf{u}'_p=\frac{\mathbf{u}_p}{U}, \quad p'_f=\frac{p_f}{\rho U^2}, \quad \text{and} p'_p=\frac{p_p}{\rho U^2}. \tag{3.17}$$

where the problem's characteristic length (L) and velocity (U) are, respectively (The same formulation is utilized for the liquid phase and the permeable medium). By inserting (3.17) into (3.1), the dimensionless Navier–Stokes equations are obtained:

$$\frac{\partial \mathbf{u}'_f}{\partial t'}+(\mathbf{u}'_f\cdot\nabla)\mathbf{u}'_f-\frac{1}{\mathrm{Re}_f}\nabla\cdot\nabla\mathbf{u}'_f+\nabla p'_f=0 \quad \text{in } \Omega_f, \tag{3.18}$$

With Re_f being the Reynolds number introduced in (3.2), the non-dimensional structure of Darcy's law (3.3) takes the following form:

$$\mathbf{u}'_p+\mathrm{Gr}_n(\nabla p'_p)=0 \quad \text{in}\,\Omega_p. \tag{3.19}$$

$$\mathrm{Gr}_n=\frac{\rho K U}{\mu L}. \tag{3.20}$$

Alternatively, the non-dimension representation of the Forchheimer equation (3.5)

takes the form:

$$\mathbf{u'}_p + \mathrm{Gr}_n \nabla p'_p = -\mathrm{Gr}_f \, |\mathbf{u'}_p| \mathbf{u'}_p \quad \text{in}\, \Omega_p, \tag{3.21}$$

The non-dimensional group is expressed as Gr_f.

$$\mathrm{Gr}_f = \frac{\rho C_F U \sqrt{K}}{\mu}. \tag{3.22}$$

The three coupling conditions (3.9), (3.10), and (3.13) at the interface are made dimensionless as

$$\mathbf{u'}_f \cdot \mathbf{n}_f = \mathrm{Gr}_n \frac{\partial p'_p}{\partial n'_p}, \tag{3.23}$$

$$p'_f - \frac{1}{\mathrm{Re}_f} \frac{\partial \mathbf{u'}_f}{\partial n'_f} \cdot \mathbf{n}_f = p'_p, \tag{3.24}$$

$$-\frac{\partial \mathbf{u'}_f}{\partial n'_f}\bigg|_\tau = \mathrm{Gr}_c \mathbf{u'}_f|_\tau, \tag{3.25}$$

where Gr_c is represented as

$$\mathrm{Gr}_c = \alpha_{BJ} \frac{L}{\sqrt{K}}. \tag{3.26}$$

The non-dimensional representation of thepenalized Navier–Stokes equations (3.15) is presented as follows:

$$\frac{\partial \mathbf{u'}}{\partial t'} + (\mathbf{u'} \cdot \nabla)\mathbf{u'} - \frac{1}{\mathrm{Re}} \nabla \cdot \nabla \mathbf{u'} + \mathrm{Gr}_i |\mathbf{u'}| \mathbf{u'} + \mathrm{Gr}_v \mathbf{u'} + \nabla p' = \mathbf{0} \quad \text{in}\, \Omega, \tag{3.27}$$

with non-dimensional groups

$$\mathrm{Re} = \frac{\rho L U}{\mu}, \quad \mathrm{Gr}_v = \frac{P_v L}{\rho U}, \quad \text{and} \quad \mathrm{Gr}_i = \frac{P_i L}{\rho}. \tag{3.28}$$

For conciseness, a non-dimensional formulation is adopted henceforth, disregard-

ing superscripts for simplicity in notation. A concise summary of the models to be examined in the following sections is presented below.

The Navier–Stokes-Darcy (NSD) mathematical model:

$$\begin{aligned}
&\frac{\partial \mathbf{u}_f}{\partial t} + (\mathbf{u}_f \cdot \nabla)\mathbf{u}_f - \frac{1}{\mathrm{Re}_f}\nabla \cdot \nabla \mathbf{u}_f + \nabla p_f = 0 && \text{in } \Omega_f,\\
&\nabla \cdot \mathbf{u}_f = 0 && \text{in } \Omega_f,\\
&-\nabla \cdot (\mathrm{Gr}_n \nabla p_p) = 0 && \text{in } \Omega_p,\\
&\mathbf{u}_f \cdot \mathbf{n}_f = \mathrm{Gr}_n \frac{\partial p_p}{\partial n_p} && \text{on } \Gamma,\\
&p_f - \frac{1}{\mathrm{Re}_f}\frac{\partial \mathbf{u}_f}{\partial n_f} \cdot \mathbf{n}_f = p_p && \text{on } \Gamma,\\
&-\left(\frac{\partial \mathbf{u}_f}{\partial \mathbf{n_f}}\right)_\tau = Gr_c(\mathbf{u}_f)_\tau && \text{on } \Gamma.
\end{aligned} \tag{3.29}$$

The Navier–Stokes-Forchheimer (NSF) mathematical model:

$$\begin{aligned}
&\frac{\partial \mathbf{u}_f}{\partial t} + (\mathbf{u}_f \cdot \nabla)\mathbf{u}_f - \frac{1}{\mathrm{Re}_f}\nabla \cdot \nabla \mathbf{u}_f + \nabla p_f = 0 && \text{in } \Omega_f,\\
&\nabla \cdot \mathbf{u}_f = 0 && \text{in } \Omega_f,\\
&\mathbf{u}_p + \mathrm{Gr}_f |\mathbf{u}_p| \mathbf{u}_p = -\mathrm{Gr}_n \nabla p_p = 0 && \text{in } \Omega_p,\\
&\nabla \cdot \mathbf{u}_p = 0 && \text{in } \Omega_p,\\
&\mathbf{u}_f \cdot \mathbf{n}_f = -\mathbf{u}_p \cdot \mathbf{n}_p && \text{on } \Gamma,\\
&p_f - \frac{1}{\mathrm{Re}_f}\frac{\partial \mathbf{u}_f}{\partial n_f} \cdot \mathbf{n}_f = p_p && \text{on } \Gamma,\\
&-(\frac{\partial \mathbf{u}_f}{\partial n_f})_\tau = Gr_c(\mathbf{u}_f)_\tau && \text{on } \Gamma.
\end{aligned} \tag{3.30}$$

The penalization mathematical model:

$$\begin{aligned}
&\frac{\partial \mathbf{u}}{\partial t} + (\mathbf{u} \cdot \nabla)\mathbf{u} - \frac{1}{\mathrm{Re}}\nabla \cdot \nabla \mathbf{u} + \mathrm{Gr}_i |\mathbf{u}| \mathbf{u} + \mathrm{Gr}_v \mathbf{u} + \nabla p = 0 && \text{in } \Omega,\\
&\nabla \cdot \mathbf{u} = 0 && \text{in } \Omega.
\end{aligned} \tag{3.31}$$

It is important to note that all physical variables are expressed in dimensionless

form. Suitable boundary conditions for the system will be subsequently introduced in Section 3.1.6.

3.1.6 Boundary Conditions

To illustrate the boundary conditions, we focus on a specific two-dimensional problem for simplicity, although the concepts presented can be readily extended to more general scenarios. A horizontal fluid flow is considered over a saturated porous medium. Fluid enters the domain through the inlet boundary (γ_1) and exits through porous and fluid outlets (γ_1 and δ_3). Other boundaries are assumed to be impermeable. No-slip boundary condition is imposed on boundary γ_2, while a slip condition is applied on boundaries δ_1 and δ_2. The characteristic length scale for non-dimensionalization is chosen as the height of the fluid channel (L), and the characteristic velocity is taken as the maximum inlet velocity (U) In more detail, the boundary conditions applied to the NSD model (3.29) are as follows:

$$
\begin{aligned}
&\underline{\text{at } \gamma_1:} \quad \mathbf{u}_f = u_{pois}, \\
&\qquad\qquad \text{where} \quad u_{pois} = \left(y^2 - 4y, 0\right), \\
&\underline{\text{at } \gamma_2:} \quad \mathbf{u}_f = \mathbf{0}, \\
&\underline{\text{at } \gamma_3:} \quad p_f \mathbf{n}_f - \frac{1}{\mathrm{Re}_f} \frac{\partial \mathbf{u}_f}{\partial n_f} = \mathbf{0}, \\
&\underline{\text{at } \delta_1 \text{ and } \delta_2:} \quad \frac{\partial p_p}{\partial n_p} = 0, \quad \mathbf{u}_p = 0, \\
&\underline{\text{at } \delta_3:} \quad p_p = 0.
\end{aligned}
\tag{3.32}
$$

The interface condition is given as:

$$
\underline{\text{at } \Gamma:} \quad \mathbf{u}_f = \mathbf{u}_p.
$$

The function $\mathbf{u}_{\text{pois}}$ defines a given Poiseuille velocity profile at γ_1. Identical boundary conditions are applied for the NSF problem (3.30), with (3.32)4 being substituted by.

$$\mathbf{u}_p \cdot \mathbf{n}_p = 0 \quad \text{on } \delta_1 \cup \delta_2.$$

The imposition of boundary conditions for the PE problem (3.31) requires a slight modification.

$$\begin{aligned}
&\mathbf{u} = \mathbf{u}_{\text{pois}} && \text{on } \gamma_1, \\
&\mathbf{u} = \mathbf{0} && \text{on } \gamma_2, \\
&p\mathbf{n} - \frac{1}{\text{Re}}\frac{\partial \mathbf{u}}{\partial n} = \mathbf{0} && \text{on } \gamma_3, \\
&\mathbf{u} \cdot \mathbf{n} = 0 && \text{on } \delta_1 \cup \delta_2, \\
&(\frac{\partial \mathbf{u}}{\partial n})_\tau = 0 && \text{on } \delta_1 \cup \delta_2, \\
&p\mathbf{n} - \frac{1}{\text{Re}}\frac{\partial \mathbf{u}}{\partial n} = \mathbf{0} && \text{on } \delta_3.
\end{aligned} \tag{3.33}$$

The definitions and boundaries pertaining to Γ, γ_1, γ_2, γ_3, and δ_1, δ_2, and δ_3 are shown in the image below, which also clearly illustrates each term's function. Boundary condition $(3.32)_5$ has been modified to $(3.33)_6$, as the stress on bound-

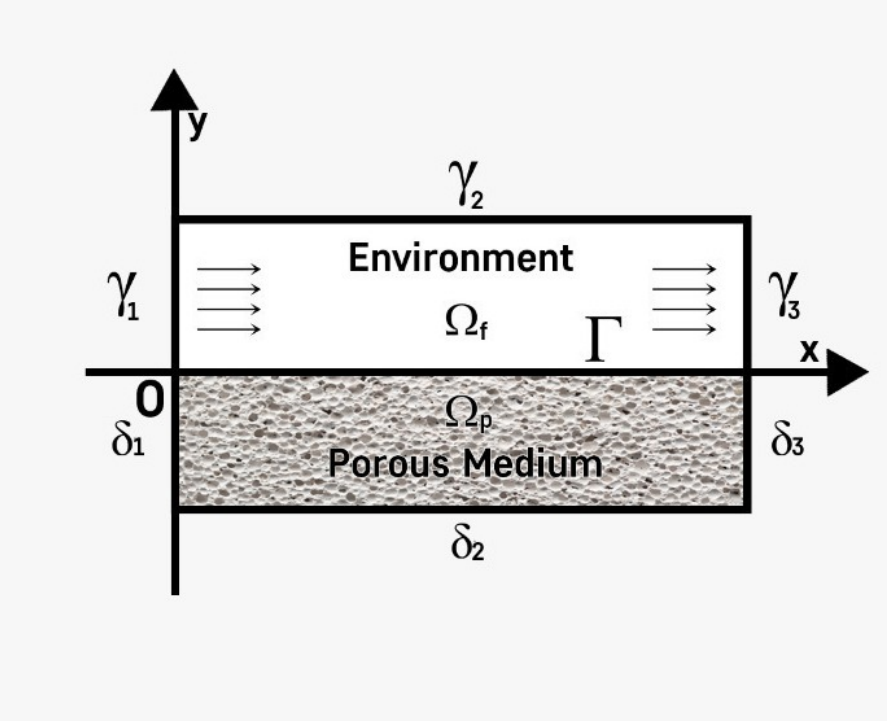

FIGURE 3.2: Schematic two-dimensional problem geometry

ary δ_3 is not solely determined by pressure in the latter case, but by the full

Cauchy stress tensor. Furthermore, boundary condition $(3.32)_4$ has been replaced by $(3.33)_4$ and $(3.33)_5$. This modification is necessary because, based on Darcy's law, $(3.32)_4$ corresponds to the zero normal velocity condition $(3.33)_4$, while $(3.33)_5$ is stated to guarantee the well-posedness of the mathematical problem.

For considered problem, the initial condition in the fluid domain Ω_f is assumed to be a fully developed Poiseuille flow profile, i.e., $\mathbf{u}_f(t=0) = \mathbf{u}_{\text{pois}}$ in Ω_f. In contrast, the porous medium is initially assumed to be at rest with no flow. The simulation commences by abruptly removing a hypothetical rigid barrier separating the fluid and porous domains, thereby allowing the fluid to infiltrate the porous bed.

3.2 Navier-Stokes Forchheimer Thermal Flow Model in Porous Media

Let us examine a region with finite boundaries Ω be a subset of $\mathbb{R}^d$ $(d = 2, 3)$ split in to two domains:

$$\Omega = \Omega_f \cup \Omega_p, \text{and} \Omega_f \cap \Omega_p = \emptyset.$$

In this study, Ω_f represents the fluid domain, while Ω_p denotes the domain occupied by the saturated porous medium. The interface between these two distinct domains is defined as $\Gamma = \Omega_f \cap \Omega_p$, as illustrated in Figure 1. From a physical perspective, Γ corresponds to the contact surface between the unrestricted fluid and the permeable medium.

3.2.1 The Navier-Stokes Equations

Within Ω_f, the behavior of a fluid of constant density is described by the equations of fluid motion, at all times, $t > 0$.

$$\rho\left(\frac{\partial \mathbf{u}_f}{\partial t} + (\mathbf{u}_f \cdot \nabla)\mathbf{u}_f\right) - \mu\nabla \cdot \nabla \mathbf{u}_f + \nabla p_f = \mathbf{0} \quad \text{in } \Omega_f, \tag{3.34}$$

$$\rho C_p \left(\frac{\partial \theta}{\partial t} + \mathbf{u}_f \cdot \nabla \theta \right) = K \nabla^2 \theta \quad \text{in } \Omega_f, \tag{3.35}$$

$$\nabla \cdot \mathbf{u}_f = 0 \quad \text{in } \Omega_f. \tag{3.36}$$

At which $\mathbf{u}_f$ and $\mathbf{p}_f$ symbolize the fluid's flow speed and stress, while ρ and μ represent its mass density and resistance to deformation, respectively. Furthermore, θ denotes the temperature, and κ signifies the thermal conductivity. We assume that the body is free from external loads, such as gravity, friction, or any other type of external force. We have used $\nabla \cdot \nabla$, ∇, and $\nabla \cdot$ to represent, respectively, the Laplace operator, the gradient, and the divergence with respect to the spatial coordinates. Additionally, we note that

$$(\mathbf{v} \cdot \nabla)\mathbf{w} = \sum_{i=1}^{d} v_i \frac{\partial \mathbf{w}}{\partial x_i},$$

for every vector function $\mathbf{v} = (v_1, \ldots, v_d)$ and $\mathbf{w} = (w_1, \ldots, w_d)$.

3.2.2 Filtration through the Permeable Domain

Darcy's law describes fluid flow through saturated porous media, assuming an average velocity that represents sample volumes much larger than individual pores. Darcy's law establishes a linear proportional relationship between the seepage velocity Here we have the $\mathbf{u}_p$ vector and the hydraulic pressure $\mathbf{p}_p$ in a permeable medium.

$$\mathbf{u}_p = -\frac{K}{\mu} \nabla p_p \quad \text{in } \Omega_p. \tag{3.37}$$

The Darcy law, which relates seepage velocity to pressure, involves two key parameters: μ (dynamic viscosity coefficient, previously defined) and k (permeability coefficient). It was first discovered by Darcy through a landmark experiment [53], later mathematically calculated from the NSE using homogenization techniques [54, 55]. Permeability coefficient (K) ranges from $10^{-5} m^2$ (highly porous materials)

to $10^{-20}m^2$ (low-permeability soils/rocks). For non-isotropic media, k is replaced by permeability tensor $\mathbf{k}$, which considers directional dependence.Seepage velocity increases lead to a smooth transition to non-linear drag. A pore-scale Reynolds number, analogous to the Navier-Stokes equations, helps assess the impact of inertial effects in the fluid flow through the porous medium.

The Reynolds number is a dimensionless quantity that helps characterize the nature of fluid flow, and in this context, it's used to understand the importance of inertial effects in the flow through porous media.

$$\mathrm{Re}_p = \frac{\rho U \delta}{\mu}. \tag{3.38}$$

So, if we see δ in an equation or expression, it's likely referring to the size of the pores in the medium, which can affect the flow and transport of fluids through the medium. The Darcy law is applicable and reliable for pore-scale Reynolds numbers $\mathrm{Re} < 1$ (see [56–58]). However, for Reynolds numbers $\mathrm{Re} > 1$, inertial effects become significant, and a more general model, such as the nonlinear Forchheimer equation [59] is required to accurately account for these effects.

$$\nabla p_p = -\frac{\mu}{K}\mathbf{u}_p - \frac{\rho C_F}{\sqrt{K}}|\mathbf{u}_p|\mathbf{u}_p \quad \text{in } \Omega_p. \tag{3.39}$$

Forchheimer equation adds inertial resistance coefficient C_f to Darcy law, with transition at $1 < \mathrm{Re}_p < 10$. In a broader sense, the term $|\mathbf{u}_p|^{\alpha}\,\mathbf{u}_p$ which is non-linear correction term, where α ranges between 1 and 2, can be viewed as modifications to Darcy's law. Comprehensive analyses of their physical interpretation are available in reference [60, 61]. Just like Darcy's law, the Forchheimer equation can be obtained by homogenizing the Navier-Stokes equations see [62]. Together with the continuity equation, this completely defines the filtration model.

$$\nabla.\mathbf{u}_p = 0 \quad \text{in } \Omega_p. \tag{3.40}$$

When coupled with Darcy's equation (4), this results in the following elliptic equa-

tion that involves only the pressure:

$$-\nabla \cdot \left(\frac{K}{\mu} \nabla p_p \right) = 0 \quad \text{in } \Omega_p. \tag{3.41}$$

If Equation 8 is solved exclusively in Ω_p , the velocity can be obtained through Darcy's law (Equation 4).

3.2.3 The Condition Across the Interface

To model the transfer of heat from the human body to the external environment through a porous medium, we need to establish appropriate conditions between the Navier-Stokes, Darcy and thermal energy equations at their shared interface, denoted by Γ. This coupling enables the exchange of heat and momentum across the interface, allowing for a comprehensive understanding of the thermal and fluid dynamics involved.

1. Preservation of the perpendicular aspect of energy/ heat and velocity:

$$\theta_f \cdot \mathbf{n}_f = -\theta_p \cdot \mathbf{n}_p \quad \text{on } \Gamma, \tag{3.42}$$

where θ_f and θ_p represent thermal energies and $\mathbf{n}_f$, $\mathbf{n}_p$ represent unit normal energies to $\partial\Omega_f$ and $\partial\Omega_p$ respectively: where $\mathbf{n}_f$ = - $\mathbf{n}_p$ Now from equation 2:

$$\rho C_p \left(\frac{\partial \theta}{\partial t} + \mathbf{u}_f \cdot \frac{\partial \theta_p}{\partial n_p} \right) = K \frac{\partial^2 \theta_p}{\partial \mathbf{n}_p^2} \theta \quad \text{on } \Gamma, \tag{3.43}$$

$$\mathbf{u}_f \cdot \mathbf{n}_f = -\mathbf{u}_p \cdot \mathbf{n}_p \quad \text{on } \Gamma, \tag{3.44}$$

and Equation 4 can be written as

$$\mathbf{u}_f \cdot \mathbf{n}_f = \frac{K}{\mu} \frac{\partial p_p}{\partial n_p} \quad \text{on } \Gamma. \tag{3.45}$$

2. Effect of energy from body to porous medium:

$$\theta_b \cdot \mathbf{n}_b = -\theta_p \cdot \mathbf{n}_p \quad \text{on } \Gamma, \tag{3.46}$$

where θ_b and θ_b represent thermal energies on *Gamma*

$$\rho C_p \left(\frac{\partial \theta}{\partial t} + \mathbf{u}_f \cdot \frac{\partial \theta_b}{\partial n_b} \right) = K \frac{\partial^2 \theta_b}{\partial \mathbf{n}_b^2} \theta \quad \text{on } \Gamma. \tag{3.47}$$

3.2.4 Dimensionless Formulations

To facilitate a comparison between the models, we will express them in dimensionless form. To this end, we introduce the dimensionless variables provided below.

$$\mathbf{X}' = \frac{\mathbf{x}}{L}, \quad t' = \frac{U}{L}t, \quad \mathbf{u}'_f = \frac{\mathbf{u}_f}{U}, \quad \mathbf{u}'_p = \frac{\mathbf{u}_p}{U}, \quad p'_f = \frac{p_f}{\rho U^2}, \quad p'_p = \frac{p_p}{\rho U^2}, \quad \theta' = \frac{\theta - \theta_\infty}{\theta_w - \theta_\infty}.$$

Here U and L are respectively a velocity and length for this case. By substituting above dimensionless variables in (3.34) ; we obtain dimensionless formulation:

$$\begin{aligned}
(3.34) \quad \Longrightarrow \quad \rho \frac{\partial \mathbf{u}_f}{\partial t} + (\mathbf{u}_f \cdot \nabla)\mathbf{u}_f - \mu \nabla \cdot \nabla \mathbf{u}_f + \nabla p_f = 0 \quad \text{in } \Omega_f, \\
\frac{\partial \mathbf{u}_f}{\partial t} = \frac{\partial U \mathbf{u}'_f}{\partial (\frac{L}{U} t')} = \frac{U^2}{L} \frac{\partial \mathbf{u}'_f}{\partial t'}, \\
(\mathbf{u}_f \cdot \nabla)\mathbf{u}_f = (U \mathbf{u'}_f \cdot \frac{\partial}{\partial x}) U \mathbf{u}_f = \frac{U^2}{L} (\mathbf{u}'_\mathbf{f} . \nabla) \mathbf{u}'_\mathbf{f}, \\
\nabla \cdot \nabla \mathbf{u}_f = \frac{\partial^2 \mathbf{u_f}}{\partial x^2} = \frac{U}{L^2} \frac{\partial^2 \mathbf{u}'_\mathbf{f}}{\partial x'^2}, \\
\nabla p_f = \frac{\partial \rho U^2 p'_f}{\partial x} = \rho \frac{U^2}{L} \nabla . p'_f.
\end{aligned}$$

where,

$$\nu = \frac{\mu}{\rho}; \quad \text{and} \quad Re = \frac{\rho U L}{\mu}.$$

$$\begin{aligned}
&\rho \left(\frac{U^2}{L} \frac{\partial \mathbf{u'}_f}{\partial t'} + \frac{U^2}{L} (\mathbf{u'}_f \cdot \nabla) \mathbf{u'}_f \right) - \mu \frac{U}{L^2} \frac{\partial^2 \mathbf{u'}_f}{\partial x'^2} + \rho \frac{U^2}{L} \nabla p'_f = 0, \\
&\frac{\partial \mathbf{u'}_f}{\partial t'} + (\mathbf{u'}_f \cdot \nabla) \mathbf{u'}_f - \frac{\mu Re}{U \rho L} \nabla \cdot \nabla \mathbf{u'}_f + \nabla p'_f = 0.
\end{aligned}$$

$$\frac{\partial \mathbf{u}'_f}{\partial t'} + (\mathbf{u}'_f \cdot \nabla)\mathbf{u}'_f - \frac{1}{\mathrm{Re}_f}\nabla \cdot \nabla \mathbf{u}'_f + \nabla p'_f = 0 \quad \text{in } \Omega_f. \tag{3.48}$$

The Reynolds number in the fluid system is expressed as Re_f

$$\mathrm{Re}_f = \frac{\rho U L}{\mu}.$$

The Reynolds number, a dimensionless quantity, is a vital factor in fluid dynamics, helping to predict flow patterns in diverse situations. It gauges the relative influence of inertial forces compared to viscous forces within the fluid. A low Reynolds number indicates that viscous forces dominate, leading to smooth, laminar flow, while a high Reynolds number suggests that inertial effects are stronger, often resulting in turbulent flow. Understanding the Reynolds number is essential for determining the stability and nature of fluid motion in engineering and natural systems. The Navier–Stokes equations effectively simulate laminar flows characterized by relatively low Reynolds numbers. The parameters U and L represent the fundamental velocity and length scales within the flow. These are used to compute the Reynolds number $\mathrm{Re} = \frac{UL}{\nu}$, which serves as a key indicator of the flow regime. At elevated Reynolds numbers, the flow transitions from a smooth, orderly (laminar) behavior to a chaotic and unstable turbulent regime. Capturing this transition accurately is crucial for realistic modeling of many physical systems.

The dimensionless form of the thermal energy in eqn (3.35) becomes

$$\begin{aligned}
(3.35) \quad \Longrightarrow \quad & \rho C_p \left(\frac{\partial \theta}{\partial t} + \mathbf{u}_f \cdot \nabla \theta \right) = K \nabla^2 \theta, \\
& \rho C_p \left(\frac{U}{L}\frac{\partial \theta}{\partial t'} + U \mathbf{u}'_f \cdot \frac{1}{L}\nabla \theta \right) = K \frac{1}{L^2}\nabla'^2 \theta, \\
& \frac{\partial \theta}{\partial t'} + \mathbf{u}'_f \cdot \nabla \theta = \frac{K}{U L \rho C_p}\nabla'^2 \theta, \\
& = \frac{\nu K}{U L \mu C_p}\nabla'^2 \theta. \\
& \frac{\partial \theta'}{\partial t'} + \mathbf{u}'_f \cdot \nabla \theta' = \frac{1}{\mathrm{Re} \cdot P_r}\nabla^2 \theta'. \qquad (3.49)
\end{aligned}$$

where

The Prandtl number (P_r) represents the ratio of momentum diffusivity to thermal diffusivity.

$$P_r = \frac{\mu C_p}{K},$$

$$\nabla \cdot \mathbf{u_f'} = 0 \quad \text{in } \Omega. \tag{3.50}$$

Dimensionless for of Darcy law in eqn (3.37) becomes

$$\begin{aligned}
(3.37) \quad \Longrightarrow \quad \mathbf{u}_p &= -\frac{k}{\mu}\nabla p_p \quad \text{in } \Omega_p, \\
U\mathbf{u'}_p &= -\frac{K}{\mu}\frac{\partial}{\partial x}p_p \quad \text{in } \Omega_p, \\
U\mathbf{u'}_p &= -\frac{K}{\mu}\frac{1}{L}\nabla.\rho U^2 p'_p, \\
\mathbf{u'_p} &= -\frac{K\rho U}{\mu L}\nabla p'_p.
\end{aligned}$$

$$\mathbf{u}'_p = -\mathrm{Gr}_n \nabla \mathbf{P}'_p.$$

Here Gr_n is represented as

$$\mathrm{Gr}_n = \frac{\rho\ KU}{\mu L}$$

The scaled version of the Forchheimer equation is formulated as shown in (3.39).

$$\begin{aligned}
(3.39) \quad \Longrightarrow \quad \nabla p_p &= -\frac{\mu}{K}\mathbf{u}_p - \frac{\rho C_F}{\sqrt{K}}|\mathbf{u}_p|\mathbf{u}_p \quad \text{in } \Omega_p, \\
\frac{1}{L}\nabla'(\rho U^2 p'_p) &= -\frac{\mu}{K}U\mathbf{u'}_p - \frac{\rho C_F}{\sqrt{k}}|U\mathbf{u'}_p|U\mathbf{u'}_p \quad \text{in } \Omega_p, \\
\mathbf{u'_p} + \frac{KU\rho}{\mu L}\nabla' p'_p &= -\frac{\rho\sqrt{K}C_F}{\mu}U|\mathbf{u'_p}|\mathbf{u'_p}.
\end{aligned}$$

$$\mathbf{u}'_p + \mathrm{Gr}_f \left|\mathbf{u}'_p\right| \mathbf{u}'_p = -\mathrm{Gr}_n \nabla \mathbf{P}'_p,$$

where

$$\mathrm{Gr}_f = \frac{\rho C_F U\sqrt{K}}{\mu}.$$

The interface condition are likewise expressed in dimensionless form, obtaining

$$\begin{aligned}
(3.45) \quad \Longrightarrow \quad \mathbf{u}_f \cdot \mathbf{n}_f &= \frac{K}{\mu}\frac{\partial p_p}{\partial n_p} \quad \text{on } \Gamma, \\
U\mathbf{u'}_f \cdot \mathbf{n}_f &= \frac{K}{\mu}\rho U^2 \frac{\partial p'_p}{\partial n_p} \quad \text{on } \Gamma.
\end{aligned}$$

$$\mathbf{u}'_f \cdot \mathbf{n}_f = \mathrm{Gr}_n \frac{\partial\ P'_p}{\partial n'_p}. \tag{3.51}$$

$$(3.10) \quad \Longrightarrow \ p_f - \mu \frac{\partial \mathbf{u}_f}{\partial n_f} \cdot \mathbf{n}_f = p_p \quad \text{on } \Gamma,$$

$$\rho U^2 p'_f - \mu U \frac{\partial \mathbf{u}'_f}{\partial n_f} \cdot \mathbf{n}_f = \rho U^2 p'_p \quad \text{on } \Gamma.$$

$$P'_f \frac{1}{\mathrm{Re}_f} \frac{\partial \mathbf{u}'_f}{\partial n'_f} \cdot \mathbf{n}_f = P'_p. \tag{3.52}$$

$$(3.11) \quad \Longrightarrow \ -(\frac{\partial \mathbf{u}_f}{\partial n_f})_{\boldsymbol{\tau}} = \frac{\alpha_{BJ}}{\sqrt{K}}(\mathbf{u}_f - \mathbf{u}_p)_\tau \quad \text{on } \Gamma.$$

$$-(\frac{U}{L}\frac{\partial \mathbf{u}'_f}{\partial n_f})_{\boldsymbol{\tau}} = \frac{\alpha_{BJ}}{\sqrt{K}}(U\mathbf{u}'_f - U\mathbf{u}'_p)_\tau \quad \text{on } \Gamma.$$

$$-\left(\frac{\partial \mathbf{u}'_f}{\partial n'_f}\right)_\tau = \mathrm{Gr}_c \left(\mathbf{u}'_f\right)_\tau. \tag{3.53}$$

Here Gr_c is defined by

$$\mathrm{Gr}_c = \frac{\alpha_{\beta \mathrm{JL}}}{\sqrt{K}}. \tag{3.54}$$

- Navier-Stokes, thermoenergy/Darcy model:

$$\begin{aligned}
&\frac{\partial \mathbf{u}_f}{\partial t} + (\mathbf{u}_f \cdot \nabla)\mathbf{u}_f - \frac{1}{\mathrm{Re}_f}\nabla \cdot \nabla \mathbf{u}_f + \nabla p_f = 0 && \text{in } \Omega_f,\\
&\frac{\partial \theta}{\partial t} + \mathbf{u}_f \cdot \nabla \theta = \frac{1}{\mathrm{Re} \cdot P_r}\nabla^2 \theta && \text{in } \Omega_f,\\
&\nabla \cdot \mathbf{u}_f = 0 && \text{in } \Omega_p,\\
&-\nabla \cdot (\mathrm{Gr}_n \nabla \mathbf{p}_p) = 0 && \text{in } \Omega_p,\\
&\mathbf{u}_f \cdot \mathbf{n}_f = \mathrm{Gr}_n \frac{\partial p_p}{\partial n_p} && \text{on } \Gamma,\\
&p_f \frac{1}{\mathrm{Re}_f}\frac{\partial \mathbf{u}_f}{\partial n_f} \cdot \mathbf{n}_f = p_p && \text{on } \Gamma,\\
&-\left(\frac{\partial \mathbf{u}_f}{\partial n_f}\right)_\tau = \mathrm{Gr}_c \left(\mathbf{u}_f\right)_\tau && \text{on } \Gamma.
\end{aligned} \tag{3.55}$$

- Navier-Stokes,Thermal energy/Forchheimer model:

$$
\begin{aligned}
&\frac{\partial \mathbf{u}_f}{\partial t} + (\mathbf{u}_f \cdot \nabla)\mathbf{u}_f - \frac{1}{\mathrm{Re}_f}\nabla \cdot \nabla \mathbf{u}_f + \nabla p_f = 0 && \text{in } \Omega_f,\\
&\frac{\partial \theta}{\partial t} + \mathbf{u}_f \cdot \nabla \theta = \frac{1}{\mathrm{Re} \cdot P_r}\nabla \cdot \nabla \theta && \text{in } \Omega_f,\\
&\nabla \cdot \mathbf{u}_f = 0 && \text{in } \Omega_p,\\
&\mathbf{u}_p + \mathrm{Gr}_f \left|\mathbf{u}_p\right| \mathbf{u}_p = -\mathrm{Gr}_n \nabla \mathbf{p}_p = 0 &&\\
&\nabla \cdot \mathbf{u}_p = 0 && \text{in } \Omega_p,\\
&\mathbf{u}_f \cdot \mathbf{n}_f = -\mathbf{u}_p \cdot \mathbf{n}_p && \text{on } \Gamma,\\
&p_f \frac{1}{\mathrm{Re}_f}\frac{\partial \mathbf{u}_f}{\partial n_f} \cdot \mathbf{n}_f = p_p && \text{on } \Gamma,\\
&-\left(\frac{\partial \mathbf{u}_f}{\partial n_f}\right)_\tau = \mathrm{Gr}_c \left(\mathbf{u}_f\right)_\tau && \text{on } \Gamma.
\end{aligned}
\tag{3.56}
$$

3.2.5 Boundary Conditions

We now specify the boundary conditions, focusing on a simple two-dimensional (2D) problem for clarity, but note that our approach can be generalized to more complex scenarios. We analyze the setup in Fig. 2, where fluid flows vertically, interacting with a porous medium, with heat transfer. This configuration helps us examine the coupling between fluid motion and thermal behavior across different regions of the domain.

The boundaries are defined as follows: impermeable boundaries with no-slip condition on Γ_2, and slip conditions involving $\delta \cdot \delta_1$ and $\delta \cdot \delta_2$. These boundary types

are essential in capturing realistic flow behavior near solid walls and porous interfaces. Reference parameters include the channel height L and the maximum inlet velocity U, which are used to define key nondimensional quantities such as the Reynolds and Grashof numbers

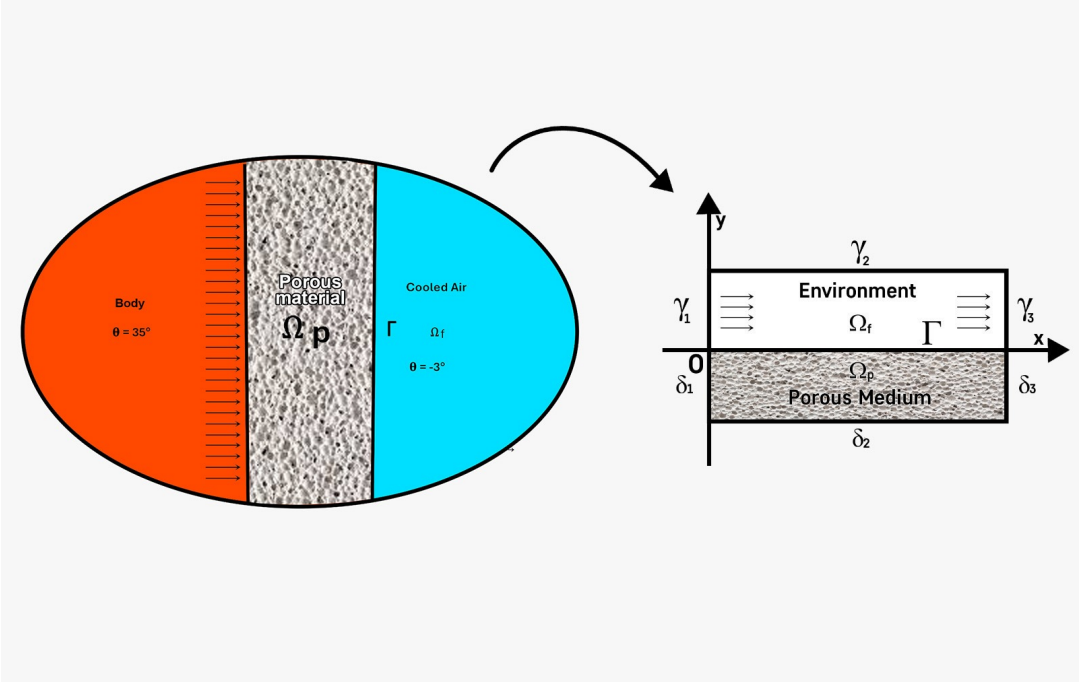

FIGURE 3.3: Schematic two-dimensional problem

The specific boundary conditions employed for the Navier-Stokes thermal energy/Darcy model are as follows:

$$
\begin{aligned}
&\underline{\text{at } \gamma_1:} \quad \mathbf{u}_f = u_{pois}, \\
&\qquad\qquad \text{where} \quad u_{pois} = \left(y^2 - 4y, 0\right), \\
&\underline{\text{at } \gamma_2:} \quad \mathbf{u}_f = \mathbf{0}, \quad \theta = 0, \\
&\underline{\text{at } \gamma_3:} \quad p_f \mathbf{n}_f - \frac{1}{\mathrm{Re}_f} \frac{\partial \mathbf{u}_f}{\partial n_f} = \mathbf{0}, \\
&\underline{\text{at } \delta_1 \text{ and } \delta_2:} \quad \frac{\partial p_p}{\partial n_p} = 0, \quad \mathbf{u}_p = 0, \\
&\underline{\text{at } \delta_2:} \quad \theta = 350, \\
&\underline{\text{at } \delta_3:} \quad p_p = 0.
\end{aligned}
\tag{3.57}
$$

The interface condition is given as:

$$
\underline{\text{at } \Gamma:} \quad \mathbf{u}_f = \mathbf{u}_p.
$$

The velocity profile, denoted by $\mathbf{u}_{\text{pois}}$, is a specified Pouiseuille profile on the boundary γ_1. The same boundary conditions are applied to the Navier-Stokes-Forchheimer problem, with equations (30) and (32) replaced

$$\mathbf{u}_p \cdot \mathbf{n}_p = 0 \quad \text{on } \delta \cdot \delta_1 \cup \delta \cdot \delta_2$$

A different configuration of boundary conditions is imposed for solving PE problem 31.

$$\begin{aligned}
&\mathbf{u} = \mathbf{u}_{\text{pois}} \quad \text{on } \gamma_1, \\
&\mathbf{u} = \mathbf{0} \quad \text{on } \gamma_2, \\
&p\mathbf{n} - \frac{1}{\text{Re}_f}\frac{\partial \mathbf{u}_f}{\partial n_f} = \mathbf{0} \quad \text{on } \gamma_3, \\
&\frac{\partial \theta}{\partial \mathbf{n}} = \theta \quad \text{on } \Gamma, \\
&\mathbf{u} \cdot \mathbf{n} = 0 \quad \text{on } \delta_1 \cup \delta_2, \\
&\left(\frac{\partial \mathbf{u}}{\partial n}\right)_\tau = 0 \quad \text{on } \delta_1 \cup \delta_2, \\
&p\mathbf{n} - \frac{1}{\text{Re}}\frac{\partial \mathbf{u}}{\partial n} = \mathbf{0} \quad \text{on } \delta_3.
\end{aligned} \tag{3.58}$$

Note that condition 32_6 has been replaced by condition 33_7, as the stress on $\delta \cdot \delta_3$ is now described by the full Cauchy stress tensor, rather than just pressure. Additionally, condition 32_5 has been split into conditions 33_5 and 33_6. Specifically, Darcy's law 32_5 implies that condition 33_5 (null normal velocity) is equivalent to condition 33_6, while condition 33_5 has been added to ensure the problem's well-posedness.

Chapter 4

Finite Element Formulations and Algorithms

For partial differential equation problems, the Finite Element Method (FEM) is a standard numerical method, particularly in fields like engineering and applied sciences. It divides a complex domain into smaller, simpler parts called finite elements, allowing for local approximation of the solution. The method uses shape functions to represent the solution within each element, ensuring overall accuracy and across the domain. FEM is especially effective for handling irregular geometries and complex boundary conditions, making it indispensable in structural analysis, fluid dynamics, and heat transfer simulations. Its adaptability and precision have made it a fundamental tool in modern engineering.
This section discusses the finite element approximation for the coupled problems analyzed in Sections 3.1.5–3.2.6 and proposes an iterative solution method utilizing a domain decomposition approach.

4.1 Division of the Spatial Domain

A structured triangulation, Triangles T make up Υ_h, which is taken into consideration for the region $\Omega_f \cup \Omega_p$ with a parameter $h > 0$. On Γ, it is assumed that

the triangulations $\Upsilon_{f,h}$ and $\Upsilon_{p,h}$, defined over subdomains Ω_f and Ω_p, are consistent, sharing edges within Γ. The assumption is also that the triangulation on Γ is quasi-uniform.[63, 64] A case in point is Fig3.3, There are numerous options for approximated solution spaces.In the framework of either the Navier-Stokes equations or the stabilized model, where $\mathbf{W}_h$ and Q_h represent the approximated solution spaces approximating the velocity and pressure fields, correspondingly, a non-negative constant $\beta^* > 0$, independent of the mesh size (h), can be identified to ensure compliance with the classical inf-sup condition.

This ensures the stability of the approximated element discretization model, For the conventional inf-sup condition to be satisfied, a constant β^*, which is greater than zero, should exist and remain unaffected by h. i.e.,

$$\forall q_h \in \mathrm{Q}_h,\ \exists \mathbf{v}_h \in \mathbf{W}_h \text{ such that } \mathbf{v}_h \neq \mathbf{0}.$$

To ensure that

$$\int_D q_h \nabla \cdot \mathbf{v}_h \, d\Omega \geq \beta^* \|\mathbf{v}_h\|_{H^1(D)} \|q_h\|_{L^2(D)}.$$

Here, for Eq.(3.29) $D = \Omega_f$ and for Eq.(3.31) $D = \Omega$

We begin by introducing the discrete solution spaces to approximate the integrated Navier-Stokes, thermal energy, and Darcy model.

- W_h (velocity approximated solution space)
- Q_h (pressure approximated solution space)
- Θ_h (temperature approximated solution spaces)
- V_h (Darcy velocity approximated solution space)

The problem answer will be approximated using these spaces.

$$\mathbf{X}_{fh} = \left\{ \mathbf{v}_h \in C^0(\Omega_f) : \mathbf{v}_h\big|_T \in [\mathbf{P}_2(T)]^2 \text{ for all } T \in \Upsilon_{fh} \right\},$$

$$\mathbf{V}_{fh} = \left\{ \mathbf{v}_h \in \mathbf{X}_{fh} : \mathbf{v}_h = \mathbf{0} \text{ on } \gamma_1 \cup \gamma_2 \right\},$$

$$\theta_h = \left\{ \theta_h \in \mathbf{X}_h : \theta_h\big|_T \in [\mathbf{P}_2(T)] \text{ for all } T \in \Upsilon_{fh} \right\},$$

$$Q_{fh} = \left\{ q_h \in C^0(\Omega_f) : q_h\big|_T \in [\mathbf{P}_1(T)] \text{ for all } T \in \Upsilon_{fh} \right\},$$

and

$$W_{ph} = \left\{ q_h \in C^0(\Omega_p) : q_h\big|_T \in [\mathbf{P}_2(T)] \text{ for all } T \in \Upsilon_{ph},\ q_h = 0 \text{ on } \delta_3 \right\}.$$

.

Subsequently, the Galerkin formulation of the interconnected Navier-Stokes, thermal energy/Darcy model problem is: Find the apprximation solutions: $\mathbf{u}_{f,h}(t) \in \mathbf{X}_{f,h}$, $\theta_{fh}(t) \in Q_{fh}$, and $p_{ph} \in W_{ph}$ such that

$$\frac{\partial \mathbf{u}_f}{\partial t} + (\mathbf{u}_f \cdot \nabla)\mathbf{u}_f - \frac{1}{\mathrm{Re}_f}\Delta \mathbf{u}_f + \nabla p_f = 0 \qquad \text{in}\, \Omega_f.$$

Now, integrating the second part of the equation:

$$\int_\Omega (-\frac{1}{\mathrm{Re}_f}\Delta \mathbf{u}_f . v) d\Omega + \int_\Omega (\nabla p . v) d\Omega = 0 \quad \text{in}\, \Omega.$$

To calculate

$$\int_\Omega (-\frac{1}{\mathrm{Re}_f}\Delta \mathbf{u}_f . v) d\Omega.$$

Let

$$\nabla.(\nabla u.v) = \Delta u.v + \nabla u : \nabla v,$$
$$\implies \int \nabla.(\nabla u.v) = \int \Delta u.v + \int \nabla u : \nabla v,$$
$$\implies \int_\Omega \Delta u.v = \int_\Omega \nabla u : \nabla v - \int_\Omega \nabla.(\nabla u.v).$$

By divergence theorem:

$$\int_\Omega (-\frac{1}{\mathrm{Re}_f}\Delta \mathbf{u}.v)d\Omega = \int_\Omega (-\frac{1}{\mathrm{Re}_f}\nabla \mathbf{u}.v).nd\Gamma + \frac{1}{\mathrm{Re}_f}\int_\Omega \nabla u : \nabla v d\Gamma,$$
$$\implies = \int_\Omega (-\frac{1}{\mathrm{Re}_f}\nabla \mathbf{u}.v).nd\Gamma + \frac{1}{\mathrm{Re}_f}\int_\Omega \nabla u : \nabla v d\Gamma,$$
$$\implies = \int_\Omega (-\frac{1}{\mathrm{Re}_f}\nabla \mathbf{u}.n).vd\Gamma + \frac{1}{\mathrm{Re}_f}\int_\Omega \nabla u : \nabla v d\Gamma,$$
$$\implies \int_\Omega (\frac{1}{\mathrm{Re}_f}\frac{-\partial u}{\partial n}.v)d\Gamma = \int_\Omega (-\frac{1}{\mathrm{Re}_f}\nabla \mathbf{u}.v).nd\Gamma + \frac{1}{\mathrm{Re}_f}\int_\Omega \nabla u : \nabla v d\Gamma.$$

By using coupling conditions

$$\int_\Omega (\frac{1}{\mathrm{Re}_f}Gr_c(\mathbf{u_f})_\tau.v)d\Gamma = \int_\Omega (-\frac{1}{\mathrm{Re}_f}\nabla \mathbf{u}.v).nd\Gamma + \frac{1}{\mathrm{Re}_f}\int_\Omega \nabla u : \nabla v d\Gamma.$$

To calculate

$$\int_\Omega (\nabla p.v)d\Omega = 0 \quad \text{in}\,\Omega.$$

Let

$$\nabla(p.v) = \nabla p.v + p\nabla.v.$$

By integrating

$$\int_\Omega \nabla(p.v) = \int \nabla p.v + \int p\nabla.v,$$
$$\int_\Omega \nabla p.v = -\int p\nabla.v + \int \nabla.(pv),$$
$$= -\int_\Omega p\nabla.v + \int_\Gamma (pv).nd\Gamma.$$

$$\int_\Omega \frac{\partial \mathbf{u}_{fh}}{\partial t}\cdot \mathbf{v}_{fh}\,d\Omega + \int_{\Omega_f}((\mathbf{u}_{fh}\cdot\nabla)\mathbf{u}_{fh})\cdot\mathbf{v}_{fh}\,d\Omega_f + \int_\Omega \frac{1}{\mathrm{Re}_f}\nabla\mathbf{u}_{fh}\cdot\nabla\mathbf{v}_{fh}\,d\Omega$$
$$-\int_\Omega p_{fh}\nabla\cdot\mathbf{v}_{fh}\,d\Omega + \int_\Omega p_{ph}\mathbf{v}_{fh}\cdot\mathbf{n_f}\,d\Omega + \int_\Gamma \frac{\mathrm{Gr}_c}{Re_f}(\mathbf{u}_{fh})_\tau\cdot(\mathbf{v}_{fh})_\tau = 0 \quad \forall \mathbf{v}_{fh}\in\mathbf{V}_{fh}, \tag{4.1}$$

$$\int_{\Omega}\left(\frac{\partial\theta}{\partial t}\cdot\boldsymbol{\theta}\right)\,d\Omega+\int_{\Omega}((\mathbf{u}\cdot\nabla\theta)\boldsymbol{\theta})\,d\Omega=\frac{1}{RePr}\int_{\Gamma}\theta_{pf}\cdot\boldsymbol{\theta}\,d\Gamma-\frac{1}{RePr}\int_{\Omega}\nabla\theta:\nabla\boldsymbol{\theta}\,d\Omega. \tag{4.2}$$

$$\int_{\Omega_f}(q_{fh}\nabla\cdot\mathbf{u}_{fh})\,d\Omega_f=0\quad\forall\,q_{fh}\in Q_{fh}. \tag{4.3}$$

$$-\int_{\Omega_p}\nabla.(\mathrm{Gr}_n\nabla p_p)\cdot q_{ph}=0$$

$$-\nabla.(\mathrm{Gr}_n\nabla p.q)=-\mathrm{Gr}_n\Delta pq_n-\mathrm{Gr}_n\nabla p.\nabla q$$

$$\int_{\Omega_p}\mathrm{Gr}_n\nabla p_{ph}\cdot\nabla q_{ph}\,d\Omega_p-\int_{\Gamma}\mathbf{u}_{fh}\cdot\mathbf{n}_f q_{ph}\,d\Gamma=0\quad\forall\,q_{ph}\in W_{ph}. \tag{4.4}$$

For the Navier-Stokes, thermal energy, and Forchheimer problem (3.30), we cannot eliminate the velocity variable $\mathbf{u}_p$ in the permeable domain Ω_p as was done in the case of Darcy flow. In order to formulate (3.30's) Galerkin approximation, we need to choose a suitable family of inf-sup stable finite element spaces in Ω_p as well. Additionally, we must present Lagrange multipliers to implement the continuity condition (3.30) between the fluid as well as porous regions. The subsequent finite element spaces can be applied.

$$\mathbf{X}_h=\left\{\mathbf{v}_h\in C^0(\Omega_f):\mathbf{v}_h\big|_T\in[\mathbf{P}_2(T)]^2\forall T\in\Upsilon_h\right\},$$

$$\mathbf{V}_h=\left\{\mathbf{v}_h\in\mathbf{X}_h:\mathbf{v}_h=\mathbf{0}\text{ on }\gamma_1\cup\gamma_2\text{and}\mathbf{v_h}\cdot\mathbf{n}=0\text{on}\delta_1\cup\delta_2\right\},$$

$$\theta_h=\left\{\theta_h\in\mathbf{X}_h:\theta_h\big|_T\in[\mathbf{P}_2(T)]\text{ for all }T\in\Upsilon_{fh}\right\},$$

$$Q_h=\left\{q_h\in C^0(\Omega_):q_h\big|_T\in[\mathbf{P}_1(T)]\text{ for all }T\in\Upsilon_h\right\}.$$

The derived version of the equation (3.31) using the Galerkin method is given by:

Determine $\mathbf{u_h}(t) \in \mathbf{X_h}, p_h \in Q_h$ in a way that:

$$\int_\Omega \frac{\partial \mathbf{u}_h}{\partial t} \cdot \mathbf{v}_h \, d\Omega + \int_{\Omega_f} ((\mathbf{u}_h \cdot \nabla)\mathbf{u}_h) \cdot \mathbf{v}_h \, d\Omega_f + \int_\Omega \frac{1}{\mathrm{Re}_f} \nabla \mathbf{u}_h \cdot \nabla \mathbf{v}_h \, d\Omega$$
$$- \int_\Omega p_h \nabla \cdot \mathbf{v}_h \, d\Omega + \int_\Omega \mathrm{Gr}_v \mathbf{u}_h \cdot \mathbf{v}_h \, d\Omega + \int_\Omega \mathrm{Gr}_i |\mathbf{u}_h| \mathbf{u}_h \cdot \mathbf{v}_h \, d\Omega = 0, \quad \forall \, \mathbf{v}_h \in \mathbf{V}_h. \tag{4.5}$$

$$\int_\Omega q_h (\nabla \cdot \mathbf{u}_h) \, d\Omega = 0 \quad \forall \, q_h \in Q_h. \tag{4.6}$$

4.2 Time Discretization

We use time discretization to simulate the steady-state transition of thermal energy in a material's porous comfort layer, which is our main use case. To efficiently attain the equilibrium solution, a first-order backward Euler time-stepping method is utilized, employing a semi-implicit technique to address the non-linear convective terms in the Navier-Stokes equations. We divide the time segment into fixed steps Δt, yielding a sequence: $0 = t^0 < t^1 < \ldots < t^n < t^{n+1} < \ldots$, where $t^{n+1} - t^n = \Delta t$ for all $n \geq 0$. We use the superscript n to indicate the quantities evaluated at the time step t^n.

$$\frac{1}{\Delta t} \int_{\Omega_f} \mathbf{u}_{fh}^{n+1} \cdot \mathbf{v}_{fh} \, d\Omega_f + \int_{\Omega_f} \left((\mathbf{u}_{fh}^n \cdot \nabla) \mathbf{u}_{fh}^{n+1} \right) \cdot \mathbf{v}_{fh} \, d\Omega_f + \int_{\Omega_f} \frac{1}{\mathrm{Re}_f} \nabla \mathbf{u}_{fh}^{n+1} \cdot \nabla \mathbf{v}_{fh} \, d\Omega_f$$
$$- \int_{\Omega_f} p_{fh}^{n+1} \nabla \cdot \mathbf{v}_{fh} \, d\Omega_f + \int_\Gamma p_{ph} \mathbf{v}_{fh} \cdot \mathbf{n}_f \, d\Gamma + \int_\Gamma \frac{\mathrm{Gr}_c}{\mathrm{Re}_f} (\mathbf{u}_{fh}^{n+1})_\tau \cdot (\mathbf{v}_{fh})_\tau \, d\Gamma$$
$$= \frac{1}{\Delta t} \int_{\Omega_f} \mathbf{u}_{fh}^n \cdot \mathbf{v}_{fh} \, d\Omega_f, \quad \forall \mathbf{v}_{fh} \in \mathbf{V}_{fh}, \tag{4.7}$$

$$\int_{\Omega_f} q_{fh} \nabla \cdot \mathbf{u}_{fh}^{n+1} \, d\Omega_f = 0 \quad \forall q_{fh} \in Q_{fh}, \tag{4.8}$$

$$\int_{\Omega_p} \mathrm{Gr}_n \nabla p_{ph} \cdot \nabla q_{ph}\, d\Omega_p - \int_{\Gamma} \mathbf{u}_{fh}^{n+1} \cdot \mathbf{n}_f q_{ph}\, d\Gamma = 0 \quad \forall q_{ph} \in W_{ph}. \tag{4.9}$$

4.3 An Progressive Algorithm

To tackle the Eq (4.7, 4.8, 4.9) numerically state an iterative algorithm method that alternately solves the Navier-Stokes equation in fluid domain Ω_f and the Darcy equation in permeable domain Ω_p. Since our goal is to compute the Time-independent solution, we discretize in time and adopt a scheme without sub-iterations at each time step. Instead, we follow this approach:

1. Determine $\mathbf{u_{fh}^{n+1}} \in \mathbf{X_{fh}}$, $p_{fh}^{n+1} \in Q_{fh}$ such that:

$$\begin{aligned}\frac{1}{\Delta t}\int_{\Omega_f} \mathbf{u}_{fh}^{n+1} \cdot \mathbf{v}_{fh}\, d\Omega_f + \int_{\Omega_f} \left((\mathbf{u}_{fh}^{n} \cdot \nabla)\mathbf{u}_{fh}^{n+1}\right) \cdot \mathbf{v}_{fh}\, d\Omega_f + \int_{\Omega_f} \frac{1}{\mathrm{Re}_f} \nabla \mathbf{u}_{fh}^{n+1} \cdot \nabla \mathbf{v}_{fh}\, d\Omega_f \\ - \int_{\Omega_f} p_{fh}^{n+1} \nabla \cdot \mathbf{v}_{fh}\, d\Omega_f + \int_{\Gamma} \Psi_h^n \mathbf{v}_{fh} \cdot \mathbf{n}_f\, d\Gamma + \int_{\Gamma} \frac{\mathrm{Gr}_c}{\mathrm{Re}_f} (\mathbf{u}_{fh}^{n+1})_\tau \cdot (\mathbf{v}_{fh})_\tau\, d\Gamma \\ = \frac{1}{\Delta t}\int_{\Omega_f} \mathbf{u}_{fh}^{n} \cdot \mathbf{v}_{fh}\, d\Omega_f, \quad \forall \mathbf{v}_{fh} \in \mathbf{V}_{fh},\end{aligned} \tag{4.10}$$

$$\int_{\Omega_f} q_{fh} \nabla \cdot \mathbf{u}_{fh}^{n+1}\, d\Omega_f = 0 \quad \forall q_{fh} \in Q_{fh}. \tag{4.11}$$

2.Adjust the velocity component perpendicular to the interface at Γ:

$$\{\Psi_h^{n+1} = (1-\beta)\{\Psi_h^n + \beta \mathbf{u}_{fh}^{n+1} \cdot \mathbf{n_f} \quad \text{on}\Gamma. \tag{4.12}$$

3. Determine $p_{ph}^{n+1} \in \mathbf{W_{ph}}$ such that:

$$\int_{\Omega} Gr_n \nabla p_{ph}^{n+1} \cdot \nabla q_{ph} - \int_{\Gamma} \Psi_h^{n+1} q_{ph} = 0 \quad \forall q_{ph} \in W_{ph}. \tag{4.13}$$

4. Evaluate the new pressure across Γ:

$$\{\Psi_h^{n+1} = (1-\alpha)\Psi_h^n + \alpha p_{ph}^{n+1} \quad \text{on}\Gamma \tag{4.14}$$

5. Update n and then proceed to step 1.

$$\int_{\Omega_p} \frac{Gr_n}{1+Gr_f|\mathbf{u}_p^n|}\nabla p_p^{n+1}\cdot\nabla q_{ph} - \int \Psi_h^{n+1} q_{ph} = 0 \quad \forall q_{ph} \in W_{ph}. \tag{4.15}$$

The velocity in Ω_p at time t^{n+1} can then be recovered by:

$$\mathbf{u}_p^{n+1} = \frac{-Gr_n}{1+Gr_f|\mathbf{u}_p^n|}\nabla p_p^{n+1} \quad \text{in}\Omega_p. \tag{4.16}$$

4.4 2D Model Evaluation

This section presents the numerical outcomes for a 2D test case, employing the three models reviewed in the preceding section. The results highlight how each model performs and their accuracy under the same test conditions.

A two-dimensional computational domain, as illustrated in the figure, is defined with the following parameters:

- Fluid density, $\rho = 1.184$ kg/m^3,
- Dynamic viscosity, $\mu = 1.855 \times 10^{-5}$ Pa·s,
- Permeability, $k = 3.71 \times 10^{-7}$ m^2,
- Forchheimer coefficient, $\alpha_{BJ} = 1.0$,
- Inertial coefficient, $C_f = 0.5$.

The domain extends 15 mm in the x-direction, with a fluid region height of 4 mm and a porous region height of 3 mm.

We use $L = 10^{-3}$ m and $U = 10^{-1}$ m/s as the reference characteristic quantities. The dimensionless parameters for the model, including the NSD and NSF, are:

$Re = 6.38$, $Gr_n = 2.37$, $Gr_f = 1.94$, $Gr_c = 1.64$. The dimensionless domain measures 50 units in length in the x-direction, with heights of 4 units for the fluid region and 3 units for the porous medium.

Accurate computation of the Reynolds number based on pore size (Re_p) proves challenging in this instance due to the unknown pore size (δ). Boundary conditions are specified as outlined in Section 2.6, with the inlet boundary (γ_1) characterized by a Poiseuille velocity profile given by:

$$\boldsymbol{u}_{\text{poise}} = (y(4-y), 0).$$

FreeFEM++ use of both uniform and unstructured grids, emphasizing their unique features. These grids are defined by the dimensional grid parameter $h = \frac{1}{N}$, where N denotes count of subdivisions along each boundary length. For spatial discretization, we employ $P_2 - P_1$ finite elements. Our primary focus is on the Navier-Stokes-Fourier (NSF) formulation, utilizing the method of successive approximations discussed in Section 3.3. The NSF model allows for an explicit characterization of key parameters and supports the analysis of higher Reynolds numbers Re_p within the permeable domain, extending beyond the capabilities of the Darcy model.

This figure presents the finite element solution for the steady-state NSF problem, computed on a mesh consisting of approximately 6,500 elements with $N = 3$ and a corresponding mesh size of $h = \frac{1}{3}$. It is observed that the flow abruptly enters the porous material, forming a small recirculation zone before stabilizing into a flow that is nearly horizontal.

The subsequent figure provides a visual representation of the normal velocity component across the interface, demonstrating significant filtration within the first 15 to 20 length units. The flow velocity distribution at the outlet, located 50 length units downstream in the x-direction, is also shown in the figure.

Chapter 5

Numerical Results and Discussion

To examine the values of the Grashof numbers Gr_n, Gr_f, and Gr_c, the inertial resistance coefficient C_F is first set. Ultimately, the results will be examined and presented in a table.

k	Gr_n	Gr_f	Gr_c
1×10^{-6}	6.3827	3.1914	1
1×10^{-7}	6.3827×10^{-1}	1.0092	3.1623
1×10^{-8}	6.3827×10^{-2}	0.3191	10
1×10^{-9}	6.3827×10^{-3}	0.1009	31.623
1×10^{-10}	6.3827×10^{-4}	0.0319	100
2×10^{-7}	1.2765	1.4272	2.2361
3.71×10^{-7}	2.368	1.9438	1.6418
4×10^{-7}	2.5531	2.0184	1.5811
8×10^{-7}	5.1062	2.8545	1.1180

TABLE 5.1: Tabulated results of Gr_n, Gr_f, Gr_c for the fixed $C_F = 0.5$

Likewise, we study the behavior of the Grashof number Gr_f after fixing the value of the permeability constant K at 3.71×10^{-7}. The values will then be plotted in a table for additional examination. The Figure 5.8 illustrates the significant interac-

C_F	0.5	0	0.25	0.1	0.2	0.3	0.4
Gr_f	1.94	0	0.9725	0.389	0.778	1.167	1.556

TABLE 5.2: Variation of Gr_f for fixed $K = 3.71 \times 10^{-7}$

tion between the Forchheimer coefficient (C_f) and fluid velocity. As C_f increases, the resistance to flow within the permeable medium intensifies, [48] leading to a noticeable reduction in the u-velocity profiles at the mid-section. This resistance

increases as the flow's speed rises, requiring higher pressure to maintain the same velocity, which is especially evident at higher Reynolds numbers. The analysis also accounts for the Reynolds number ($Re = 6.38$), particle Reynolds number ($Re_p = 0.005$), and the Grashof numbers ($Gr_c = 1.64$ and $Gr_n = 2.37$), emphasizing the complex interplay between flow dynamics and porous medium properties. As shown in Figure **??**, the temperature distribution at the mid-section and near the outlet of the domain changes noticeably with varying Forchheimer coefficient C_F. An increase in C_F elevates flow resistance within the porous medium, slowing fluid velocity and thereby diminishing convective heat transfer [48, 50]. In the mid-section, this results in a less pronounced temperature gradient, as heat transport by convection declines, leaving conduction as the dominant mechanism. This effect is further influenced by the set parameters, including Reynolds number ($Re = 6.38$), particle Reynolds number ($Re_p = 0.005$), Grashof number ($Gr_c = 1.64$), and natural Grashof number ($Gr_n = 2.37$), which together modulate the balance between convective and conductive heat transfer as C_F varies.

The horizontal velocity profiles illustrated in Figure 5.1 reveal the impact of varying the permeability constant K on fluid flow dynamics across distinct sections of the domain. As K increases, the flow resistance diminishes, enabling fluid to accelerate more readily within the medium, thus achieving elevated initial velocities. Higher K values enhance the fluid's initial momentum by reducing drag within the porous structure. In the mid-section, greater permeability facilitates a more uniform velocity distribution, as lower resistance encourages a steady flow profile. By contrast, lower values of K exhibit a sharper decline in velocity in this region, signifying increased resistance that restricts fluid movement.

This observed behavior aligns with Darcy's law, where velocity correlates directly with permeability. It also corresponds with findings in the literature that suggest increasing K reduces flow resistance, allowing for a smoother and more consistent velocity profile within porous domains. Additionally, as parameters such as Gr_C, Gr_n, and Gr_f vary with K, they amplify convective momentum transfer and buoyancy effects, particularly in regions where permeability is higher, further

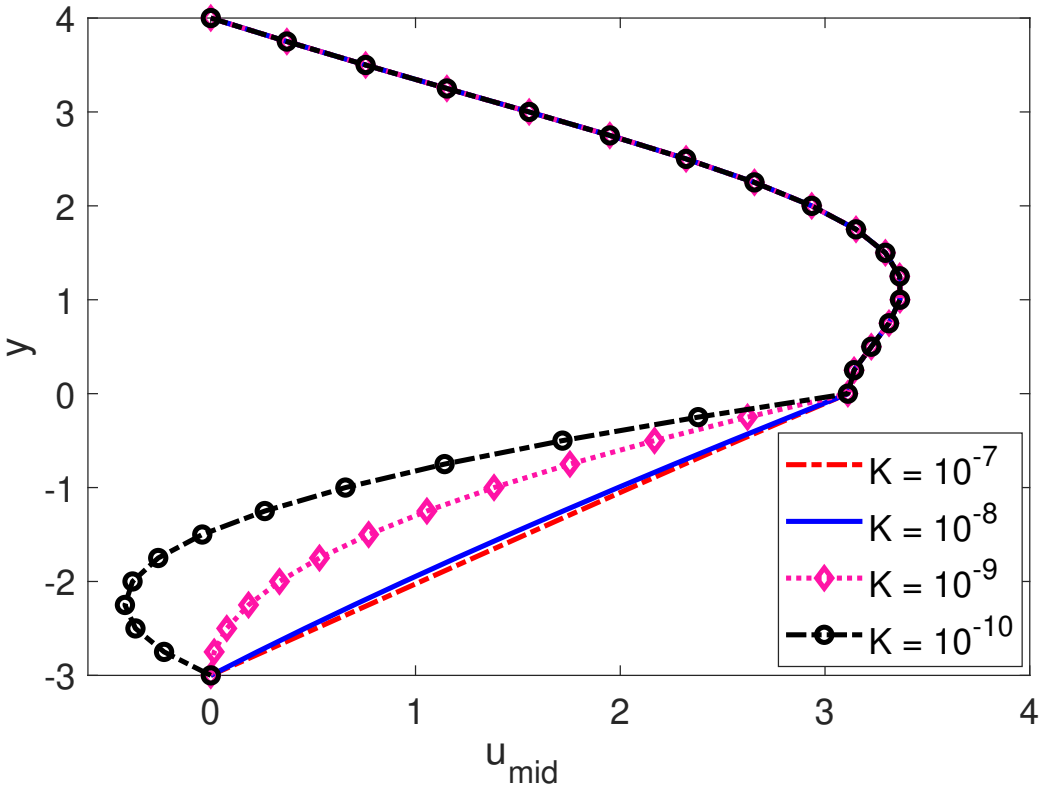

FIGURE 5.1: Horizontal velocity profiles within the medium for varying values of K. The other parameters used are: $Re = 6.38$, $Re_p = 0.005$. Note that the parameters Gr_C, Gr_n and Gr_f varies as the parameter K varies.

intensifying the flow dynamics. The temperature distribution across different sections of the porous medium, as shown in Figures 5.2 and 5.3, reveals distinct effects when the permeability K and Prandtl number Pr are varied. In Figure 5.2, for varying K, the temperature profile shows that higher K values reduce flow resistance, allowing for increased convective heat transfer and resulting in a sharper temperature gradient as heat moves quickly through the medium. Lower K values, however, create a smoother temperature profile, as the increased resistance restricts fluid flow and promotes conductive heat transfer. In the mid-section, higher K values continue to support convection, leading to a more uniform temperature distribution, while lower K values show a slower gradient due to dominance of conduction in high-resistance regions. In Figure 5.3, the temperature distribution for varying Pr shows that higher Pr values, which correspond to lower thermal diffusivity, lead to sharper temperature gradients in the mid-section as the fluid retains heat within smaller regions. Lower Pr values allow for greater thermal diffusivity, smoothing the temperature profile across the mid-section.

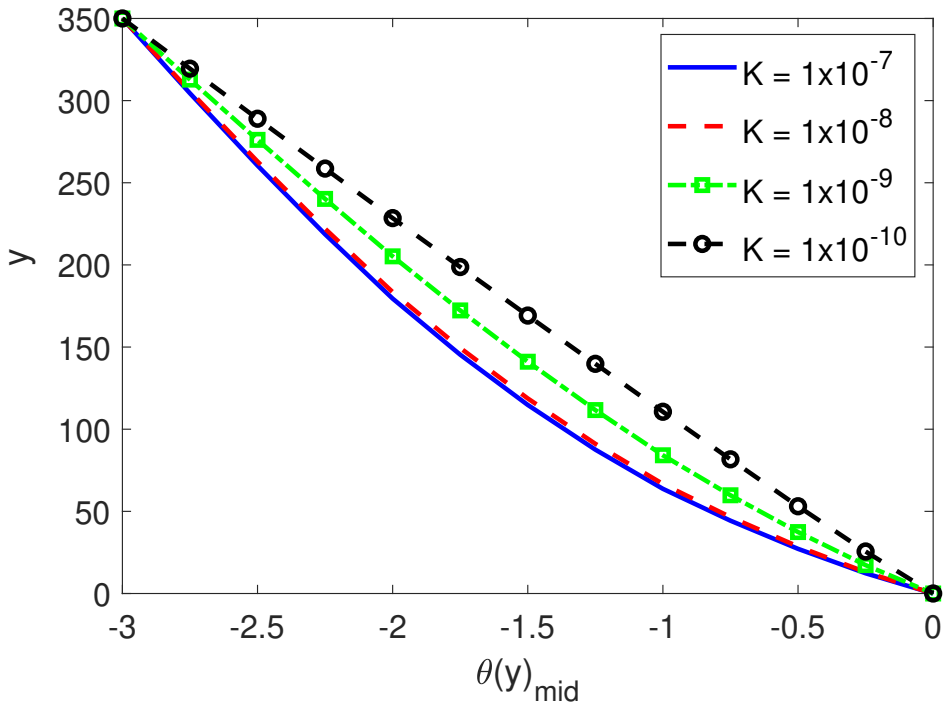

FIGURE 5.2: Temperature plot along the cross-section within the medium for varying values of K. The other parameters used are: $Re = 6.38$, $Re_p = 0.005$. Note that the parameters Gr_C, Gr_n and Gr_f varies as the parameter K varies.

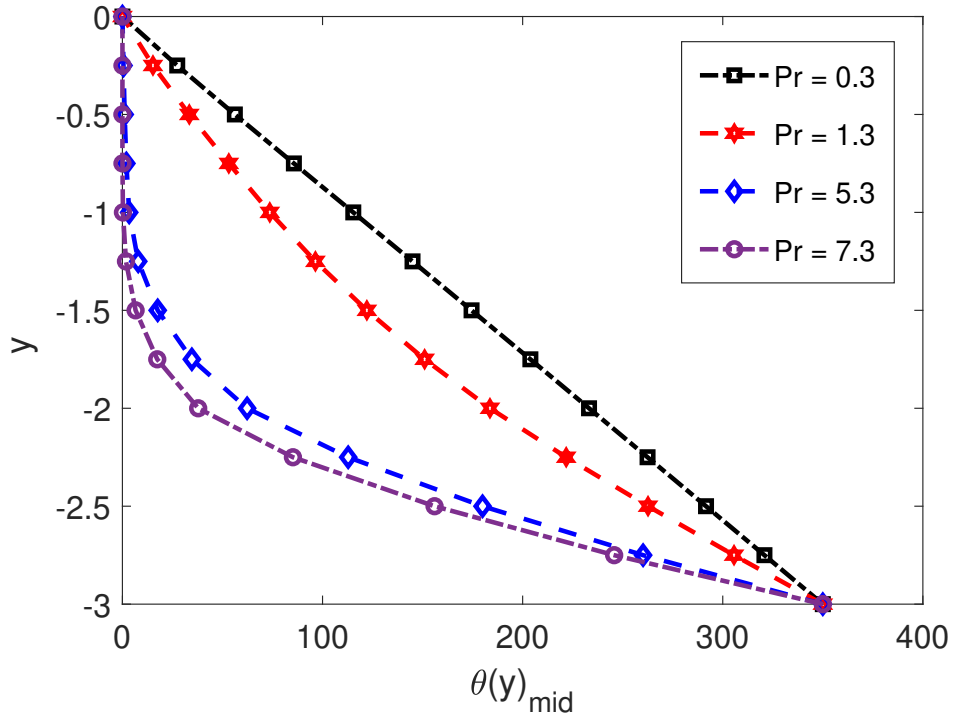

FIGURE 5.3: Temperature at mid-section of the domain for varying values of Pr. The other parameters used are: $Re = 6.38$, $Re_p = 0.005$, $Gr_C = 100$, $Gr_n = 0.0006$ and $Gr_f = 0.0319$.

These observed behaviors align with theoretical studies on heat transfer in porous media, where increased permeability enhances convection and higher Prandtl numbers constrain thermal diffusion, leading to more pronounced temperature gradients within the medium. Figure 5.4 illustrates the temperature variations at the mid-section for varying particle Reynolds numbers (Re_p). As Re_p increases, convective heat transfer enhances, leading to a faster adjustment in temperature profiles, indicating improved thermal transport. In Figure 5.5, the isotherms

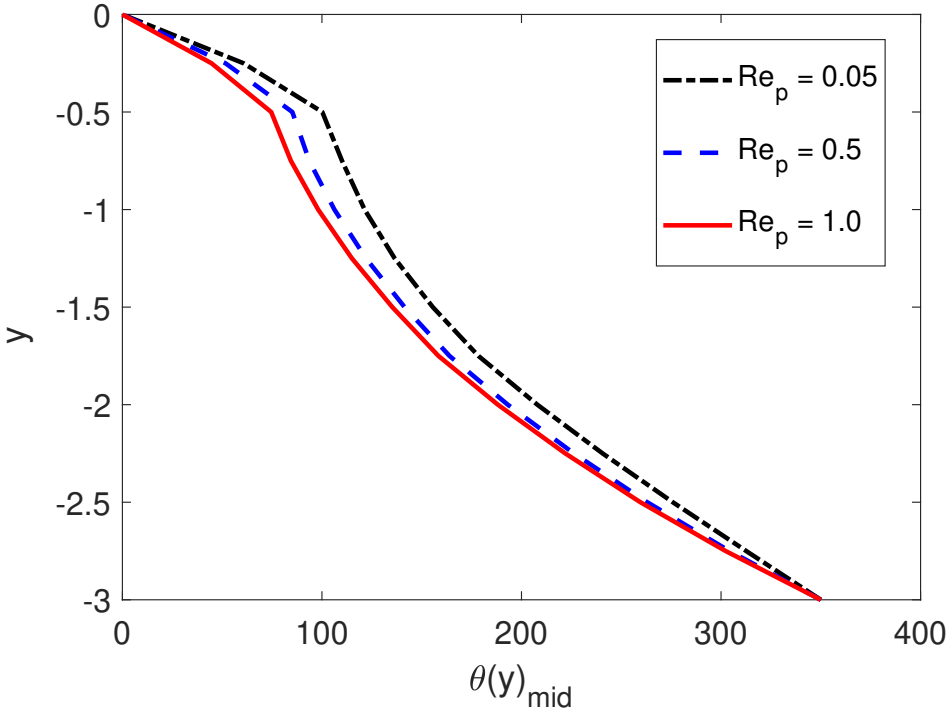

FIGURE 5.4: Temperature across mid-section for varying values of Re_p. The other parameters used are: $Re = 6.38$, $Gr_C = 100$, $Gr_n = 0.0006$ and $Gr_f = 0.0319$.

within the medium are displayed for varying values of the Prandtl number (Pr). As Pr increases, the layer of thermal influence becomes thinner and the temperature gradients within the medium become more pronounced. For lower values of Pr, the primary mode of heat transfer is convection, leading to broader isotherms that signify a more significant convective heat transfer. This behavior highlights the sensitivity of the thermal boundary layer to changes in Pr. At higher Pr values, conduction becomes more dominant near the solid boundaries, confining thermal effects to narrower regions.

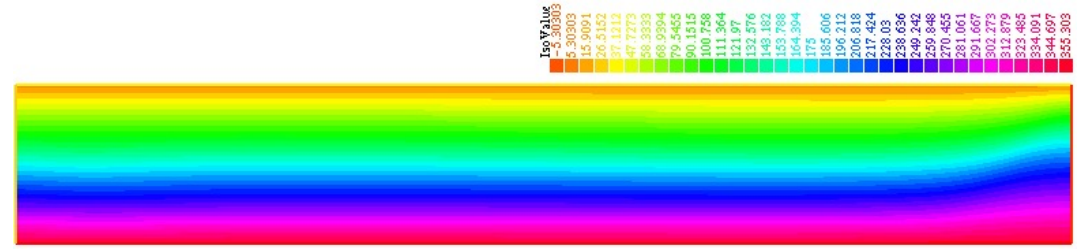

(a)

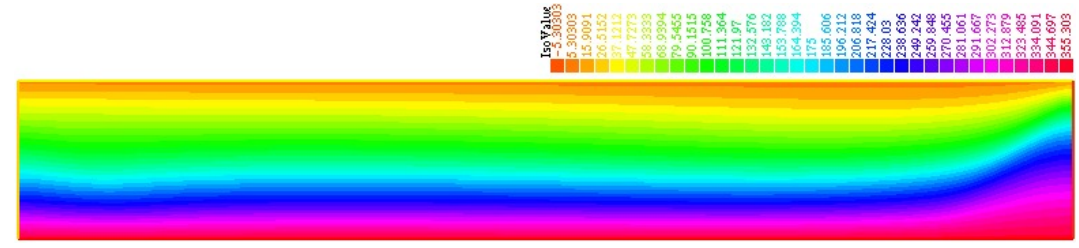

(b)

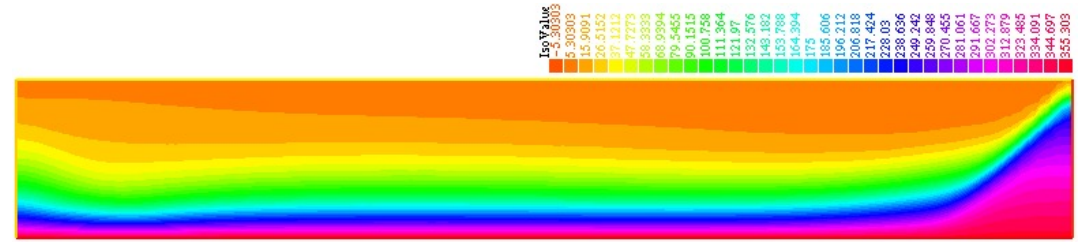

(c)

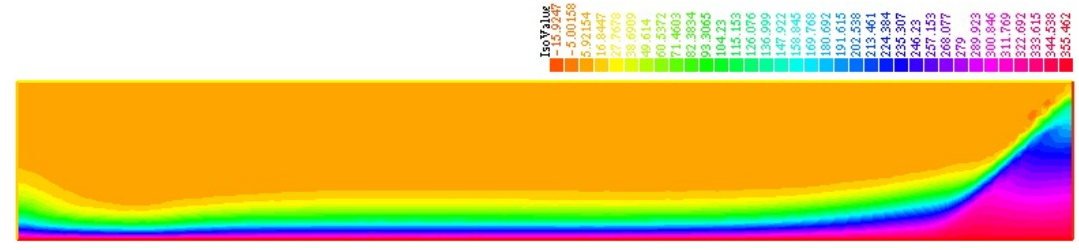

(d)

FIGURE 5.5: Isotherm contours for varying value of Prandtl number Pr. Other parameters used are: $Re = 6.38$, $Re_p = 0.005$, $Gr_c = 1.64$, $Gr_n = 2.37$, $Gr_f = 1.94$. (a) For $Pr = 0.1$ (b) For $Pr = 0.3$ (c) For $Pr = 1.3$ (d) For $Pr = 5.3$

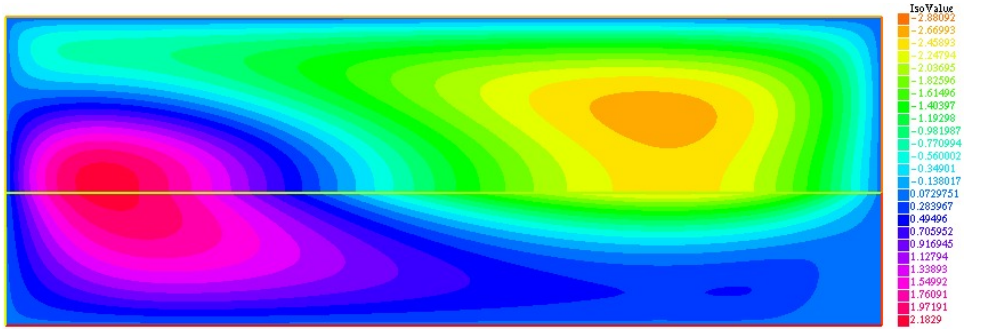

FIGURE 5.6: Streamfunction plot. Parameters used are: $Re = 6.38$, $Re_p = 0.005$, $Gr_c = 1.64$, $Gr_n = 2.37$, $Gr_f = 1.94$.

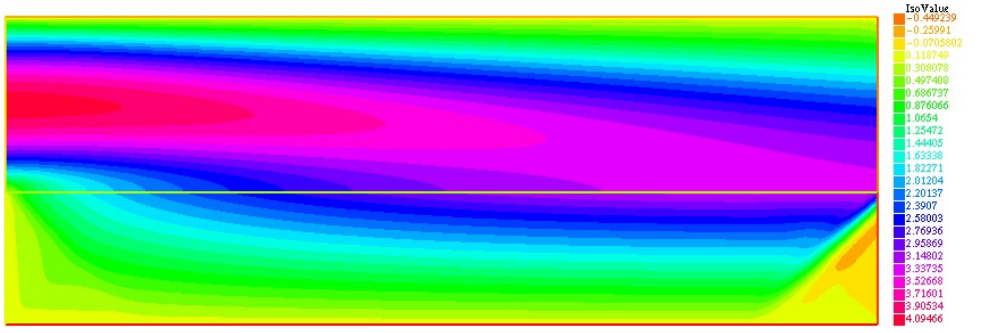

FIGURE 5.7: Horizontal velocity plot. Parameters used are: $Re = 6.38$, $Re_p = 0.005$, $Gr_c = 1.64$, $Gr_n = 2.37$, $Gr_f = 1.94$.

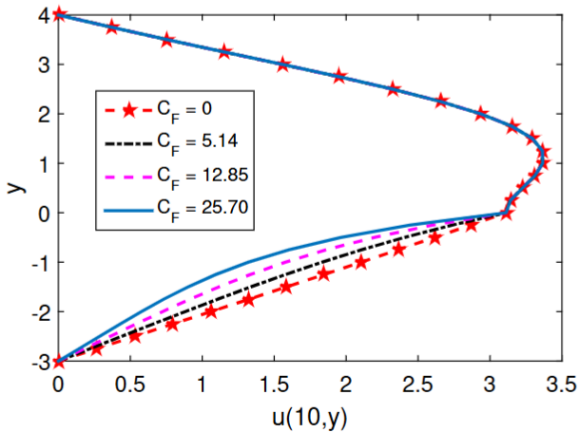

FIGURE 5.8: u-velocities at mid-section o the domain for varying Forchheimer coefficient C_F. Other parameters used are: $Re = 6.38$, $Re_p = 0.005$, $Gr_c = 1.64$, $Gr_n = 2.37$.

Chapter 6

Concluding Remarks and Perspectives for Future Research

This thesis presents a finite element-based analysis of heat transfer within a channel partially filled with a porous medium. In this regard, the dynamical properties in the porous media under consideration were modeled using a mathematical model based on the Darcy-Forchheimer model. The governing partial differential equations are integrated with the continuity requirements at the interface between the two subdomains. The weak formulation of the strong form is calculated, and the governing set of PDEs is non-dimensionalized. The FreeFEM++ open source code is then used to implement the weak formulation of the strong form of the PDEs together with the related boundary and interface constraints. Given its ability to effectively handle highly nonlinear PDEs, FreeFEM++ a mathematical tool based on finite elements was an obvious choice for our investigation. Some of the main findings of this investigation are summarized as:

- Forchheimer coefficient's interaction with fluid velocity, indicating that increasing C_F intensifies flow resistance, reducing u-velocity profiles at inlet, mid-section, and outlet.
- The temperature distribution in a porous medium changes with varying

Forchheimer coefficient (C_F) with increased C_F causing flow resistance, slowing fluid velocity, and diminishing convective heat transfer. This results in a less pronounced temperature gradient.

- By reducing flow resistance, higher permeability (K) leads to higher fluid velocities, more consistent mid-sectional profiles, and longer-lasting momentum at the exit. Lower K, on the other hand, results in more resistance, which causes greater deceleration and sharper velocity dips. According to Darcy's law, these results demonstrate how important permeability is in determining fluid dynamics and convective behavior.

- Convective heat transfer is improved by higher permeability (K), which leads to more consistent mid-section distributions, longer-lasting heat removal at the outlet, and sharper temperature gradients close to the intake. Smoother temperature profiles and more stable outlet temperatures result from the promotion of conductive heat transfer by lower K. These patterns demonstrate how heat transmission mechanisms and permeability interact in porous material.

- Lower Pr values produce smoother, more dispersed temperature profiles because of increased thermal diffusivity, whereas higher Pr values produce sharper temperature gradients because of limited thermal diffusion. These findings are consistent with theoretical heat transfer principles and show how Prandtl number affects heat distribution and retention in porous media.

- Temperature gradients inside the medium become more pronounced as Pr rises because the thermal boundary layer thins. Conversely, broader isotherms produced by lower Pr values show that convection predominates in heat transport, resulting in a more uniform dispersion of heat.

- Better convective heat transfer leads to faster temperature changes at the midsection and outlet as Re_p rises, suggesting improved thermal transport in the medium.

This analysis can be expanded to three dimensions in the future. A potential extension of this work involves applying the presented finite element method to analyze the model in a three-dimensional domain of the partially filled porous medium. The model's three-dimensional analysis will be a natural choice for observing certain more realistic phenomena that are of industrial practical importance. These results may eventually be applied to 3D models, allowing for more precise simulations of heat transmission in intricate porous media. Improved designs for systems where fluid flow and spatial temperature distribution are crucial, including in energy-efficient materials, enhanced cooling systems, and environmental applications, may result from this. We can enhance thermal management in a variety of industrial sectors and more accurately depict the intricacies of the real world by utilizing 3D effects.

Bibliography

[1] M. Muthama and S. Nicodemus. Darcy's law equation with application to underground seepage in earth dams in calculation of the amount of seepage. *American Journal of Applied Mathematics and Statistics*, pages 143–149, 2014.

[2] S. D. Ferraro, T. Falcone, M. Morabito, M. Bonafede, A. Marinaccio, C. Gao, and V. Molinaro. Mitigating heat effects in the workplace with a ventilation jacket: Simulations of the whole-body and local human thermophysiological response with a sweating thermal manikin in a warm-dry environment. *Journal of Thermal Biology*, 119:103772, 2024. ISSN 0306-4565.

[3] C. Canuto and F. Cimolin. A sweating model for the internal ventilation of a motorcycle helmet. *Computers Fluids*, 43(1):29–37, 2011. ISSN 0045-7930. Symposium on High Accuracy Flow Simulations. Special Issue Dedicated to Prof. Michel Deville.

[4] Memaon et al. Heat transfer through a higher grade forchheimer porous *cuo–h2o*-nano-medium confined between non-isothermal moving plates. *Case Studies in Thermal Engineering*, 47:103035, 2024.

[5] M. Bilal and K. Marek. Natural convection of power-law fluids in porous enclosures: Influence of porosity and thermal conditions on heat transfer. *Journal of Thermal Analysis and Calorimetry*, 149:6349–6360, 2024.

[6] F. Z. Pierre, R. D. Loubens, M. Quintard, and Y. Davit. Transition in the flow of power-law fluids through isotropic porous media. *Physical Review Letters*, 117, 2016.

[7] A. Author and B. Author. Convective flow in porous media: Transition and impact of porosity. *arXiv preprint arXiv:2409.19652*, 2024.

[8] E.M.-Paloka and A. Mikelić. The derivation of a nonlinear filtration law including the inertia effects via homogenization. *Nonlinear Analysis: Theory, Methods Applications*, 42:97–137, 2000. ISSN 0362-546X.

[9] M. Discacciati and P. Gervasio. A coupling concept for stokes-darcy systems: The icdd method. *Journal of Computational Physics*, 513:113204, 2024. ISSN 0021-9991.

[10] Z. Xin, Y. Shi, Y. Zhang, et al. A one-way coupled navier–stokes-serre model for simulating the generation and propagation of tsunami waves. *Pure and Applied Geophysics*, 181:1413–1426, 2024.

[11] F. Cimolin and M. Discacciati. Navier–stokes/forchheimer models for filtration through porous media. *Applied Numerical Mathematics*, 72:205–224, 2013. ISSN 0168-9274.

[12] A. Sirotkina, E. Fedorovich, and V. Sergeev. Model of formation and roughness calculation of the porous layer on the heated surface during nanofluids boiling. *Propulsion and Power Research*, 6(2):101–106, 2017. ISSN 2212-540X. Volume 6 Issue 2 (Special Issue) 2017.

[13] Young and A. Lewis. *University Physics with Modern Physics*. Pearson, 15 edition, 2019.

[14] White and Frank M. *Fluid Mechanics*. McGraw-Hill, 8 edition, 2016.

[15] White aand Frank M. *Fluid Mechanics*. McGraw-Hill, 8 edition, 2016.

[16] White and Frank M. *Fluid Mechanics*. McGraw-Hill, 8 edition, 2016.

[17] White and Frank M. *Fluid Mechanics*. McGraw-Hill, 8 edition, 2016.

[18] R. W. Fox, A. T. McDonald, and P. J. Pritchard. *Introduction to Fluid Mechanics*. Wiley, 9 edition, 2015.

[19] B. R. Munson, D. F. Young, and T. H. Okiishi. *Fundamentals of Fluid Mechanics*. Wiley, 7 edition, 2013.

[20] A. Bejan. *Convection Heat Transfer*. Wiley, 4 edition, 2013.

[21] Schlichting and K. Gersten. *Boundary-Layer Theory*. Springer, 8 edition, 2000.

[22] J. Bear. *Dynamics of Fluids in Porous Media*. Dover Publications, 1972.

[23] D. A. Nield and A. Bejan. *Convection in Porous Media*. Springer, 5 edition, 2017.

[24] P. Forchheimer. Wasserbewegung durch boden. *Zeitschrift des Vereins Deutscher Ingenieure*, 45:1781–1788, 1901.

[25] H. Darcy. *Les Fontaines Publiques de la Ville de Dijon*. Dalmont, Paris, 1856.

[26] L. Tartar. Incompressible fluid flow in a porous medium: convergence of the homogenization process. In E. Sánchez-Palencia, editor, *Non-Homogeneous Media and Vibration Theory*, volume 127 of *Lecture Notes in Physics*, pages 368–377. Springer, Berlin, 1980.

[27] J. Bear. *Hydraulics of Groundwater*. McGraw-Hill, New York, 1979.

[28] P. Forchheimer. Wasserbewegung durch boden. *Zeitschrift des Vereins Deutscher Ingenieure*, 45:1782–1788, 1901.

[29] M. Firdaouss, J.L. Guermond, and P. Le Quéré. Nonlinear corrections to darcy's law at low reynolds numbers. *Journal of Fluid Mechanics*, 343:331–350, 1997.

[30] M.C. Néel. Convection forcée en milieu poreux: écarts à la loi de darcy. *Comptes Rendus de l'Académie des Sciences de Paris, Série IIb*, 326:615–620, 1998.

[31] Z. Chen, S. Lyons, and G. Qin. Derivation of the forchheimer law via homogenization. *Transport in Porous Media*, 44:325–335, 2001.

[32] W. Jäger and A. Mikelic. On the boundary conditions at the contact interface between a porous medium and a free fluid. *Annali della Scuola Normale Superiore di Pisa - Classe di Scienze*, 23:403–465, 1996.

[33] G. Beavers and D. Joseph. Boundary conditions at a naturally permeable wall. *Journal of Fluid Mechanics*, 30:197–207, 1967.

[34] P. Saffman. On the boundary condition at the interface of a porous medium. *Studies in Applied Mathematics*, 1:93–101, 1971.

[35] W. Jäger and A. Mikelic. On the interface boundary condition of beavers, joseph and saffman. *SIAM Journal on Applied Mathematics*, 60:1111–1127, 2000.

[36] W. Jäger, A. Mikelic, and N. Neuss. Asymptotic analysis of the laminar viscous flow over a porous bed. *SIAM Journal on Scientific Computing*, 22: 2006–2028, 2001.

[37] M. Discacciati, E. Miglio, and A. Quarteroni. Mathematical and numerical models for coupling surface and groundwater flows. *Applied Numerical Mathematics*, 43:57–74, 2002.

[38] M. Discacciati and A. Quarteroni. Navier–stokes/darcy coupling: modeling, analysis, and numerical approximation. *Revista Matemática Complutense*, 22: 315–426, 2009.

[39] W. Layton, F. Schieweck, and I. Yotov. Coupling fluid flow with porous media flow. *SIAM Journal on Numerical Analysis*, 40:2195–2218, 2003.

[40] L. Payne and B. Straughan. Analysis of the boundary condition at the interface between a viscous fluid and a porous medium and related modelling questions. *Journal de Mathématiques Pures et Appliquées*, 77:317–354, 1998.

[41] B. Rivière and I. Yotov. Locally conservative coupling of stokes and darcy flows. *SIAM Journal on Numerical Analysis*, 42:1959–1977, 2005.

[42] J. Urquiza, D. N'Dri, A. Garon, and M. Delfour. Coupling stokes and darcy equations. *Appl. Numer. Math.*, 58:525–538, 2008.

[43] Y. Cao, M. Gunzburger, F. Hua, and X. Wang. Coupled stokes–darcy model with beavers–joseph interface boundary conditions. *Communications in Mathematical Sciences*, 8:1–25, 2010.

[44] C. Bruneau and I. Mortazavi. Numerical modelling and passive flow control using porous media. *Computers and Fluids*, 37:488–498, 2008.

[45] O. Iliev and V. Laptev. On numerical simulation of flow through oil filters. *Computational Visualisation Science*, 6:139–146, 2004.

[46] O. Iliev and D. Vasileva. On a local refinement solver for coupled flow in plain and porous media. In *Numerical Methods and Applications – 6th International Conference, NMA 2006*, Lecture Notes in Computer Science, pages 590–598, Berlin and Heidelberg, 2007. Springer. Conference held in Borovets, Bulgaria, August 20–24, 2006.

[47] K. Khadra, P. Angot, S. Parneix, and J. Caltagirone. Fictitious domain approach for numerical modelling of navier–stokes equations. *International Journal for Numerical Methods in Fluids*, 34:651–684, 2000.

[48] P. Angot. Analysis of singular perturbations on the brinkman problem for fictitious domain models of viscous flows. *Mathematical Methods in the Applied Sciences*, 22:1395–1412, 1999.

[49] H. Brinkman. A calculation of the viscous force exerted by a flowing fluid on a dense swarm of particles. *Applied Scientific Research*, 1:27–34, 1949.

[50] C. Ansys. *CFX-Solver: Theory*. Ansys Inc., 2005.

[51] C.Adapco. *Star-CCM+ User Guide*, 2007.

[52] Fluent . *Fluent User's Guide*, 2005.

[53] H Darcy. Les fontaines publiques de la ville de dijon, dalmont, paris (1856). *this original work, the ratio (k/˜) was considered as the permeability-the Darcy permeability. The permeability k should be called specific permeabi-lity*, 2007.

[54] Luc Tartar. Incompressible fluid flow in a porous medium-convergence of the homogenization process. *Non-homogeneous media and vibration theory*, 1980.

[55] A.R. Hassan, R. Maritz, and J.A. Gbadeyan. A reactive hydromagnetic heat generating fluid flow with thermal radiation within porous channel with symmetrical convective cooling. *International Journal of Thermal Sciences*, 122: 248–256, 2017. ISSN 1290-0729.

[56] Yi-P. Zhang, X.-Wei. Jiang, J. Cherry, Z.-Y. Zhang, X.-S. Wang, and L. Wan. Revisiting hydraulics of flowing artesian wells: A perspective from basinal groundwater hydraulics. *Journal of Hydrology*, 609:127714, 2022. ISSN 0022-1694.

[57] Y.-P. Zhang, X.-W. Jiang, J. Cherry, Z.-Y. Zhang, X.-S. Wang, and L. Wan. Revisiting hydraulics of flowing artesian wells: A perspective from basinal groundwater hydraulics. *Journal of Hydrology*, 609:127714, 2022. ISSN 0022-1694.

[58] O. Koit, C. Mayaud, B. Kogovšek, M. Vainu, J. Terasmaa, and A. Marandi. Surface water and groundwater hydraulics of lowland karst aquifers of estonia. *Journal of Hydrology*, 610:127908, 2022. ISSN 0022-1694.

[59] F Bertin H Lasseux, Pairoys. Fluid flow in vugular porous media. In *Poromechanics II*, pages 481–487. CRC Press, 2020.

[60] Mouaouia Firdaouss, J.-Luc Guermond, and Patrick Le Quéré. Nonlinear corrections to darcy's law at low reynolds numbers. *Journal of Fluid Mechanics*, 343:331–350, 1997.

[61] S. Liu, A. Senichault, H. Scandelli, and J. Lachaud. Experimental investigation and tomography analysis of darcy-forchheimer flows in thermal protection systems. *Acta Astronautica*, 218:147–162, 2024. ISSN 0094-5765.

[62] Zhangxin Chen, Stephen Lyons, and Guan Qin. Derivation of the forchheimer law via homogenization. *Transport in porous media*, 44:325–335, 2001.

[63] A. Quarteroni and A. Valli. *Numerical Approximation of Partial Differential Equations*. Springer, Berlin, 1994.

[64] S. Brugiapaglia, S. Micheletti, and S. Perotto. Compressed solving: A numerical approximation technique for elliptic pdes based on compressed sensing. *Computers & Mathematics with Applications*, 70(6):1306–1335, 2015. ISSN 0898-1221.